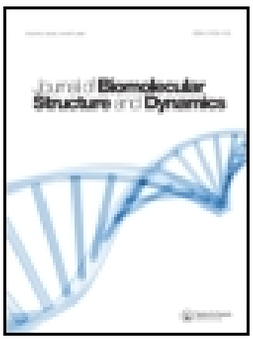

Taylor & Francis
Taylor & Francis Group

Journal of Biomolecular Structure and Dynamics

ISSN: 0739-1102 (Print) 1538-0254 (Online) Journal homepage: http://www.tandfonline.com/loi/tbsd20

Example of two novel thiocyanato bridged copper (II) complexes derived from substituted thiosemicarbazone ligand: Structural elucidation, DNA/albumin binding, biological profile analysis and molecular docking study

Niladri Biswas, Sandeepta Saha, Sumit Khanra, Arnab Sarkar, Deba Prasad Mandal, Shamee Bhattacharjee, Ankur Chaudhuri, Sibani Chakraborty & Chirantan Roy Choudhury

To cite this article: Niladri Biswas, Sandeepta Saha, Sumit Khanra, Arnab Sarkar, Deba Prasad Mandal, Shamee Bhattacharjee, Ankur Chaudhuri, Sibani Chakraborty & Chirantan Roy Choudhury (2018): Example of two novel thiocyanato bridged copper (II) complexes derived from substituted thiosemicarbazone ligand: Structural elucidation, DNA/albumin binding, biological profile analysis and molecular docking study, Journal of Biomolecular Structure and Dynamics, DOI: 10.1080/07391102.2018.1503564

To link to this article: https://doi.org/10.1080/07391102.2018.1503564

Example of two novel thiocyanato bridged copper (II) complexes derived from substituted thiosemicarbazone ligand: Structural elucidation, DNA/albumin binding, biological profile analysis and molecular docking study

Niladri Biswas[a], Sandeepta Saha[a,b] , Sumit Khanra[c], Arnab Sarkar[d], Deba Prasad Mandal[d], Shamee Bhattacharjee[d], Ankur Chaudhuri[e], Sibani Chakraborty[e], Chirantan Roy Choudhury[a]*

[a]*Department of Chemistry, West Bengal State University, Barasat, Kolkata-700126, India*

[b]*Sripur High School, Madhyamgram Bazar, Madhyamgram, Kolkata – 700130, India*

[c]*Department of Chemistry, Indian Institute of Science Education and Research, Kolkata Mohanpur - 741 246, West Bengal, India*

[d]*Department of Zoology, West Bengal State University, Barasat, Kolkata-700126, India*

[e]*Department of Microbiology, West Bengal State University, Barasat, Kolkata-700126, India*

* Corresponding author:

Tel: + 91-9836306502

Fax: +91-33-2524-1577

Email: crchoudhury2000@yahoo.com

Abstract

Two novel copper (II) substituted thiosemicarbazone Schiff base complexes $[Cu(L_1)(\mu\text{-}SCN)]_n(NO_3)_2$ (**1**) and $[Cu_2(\mu\text{-}SCN)(SCN)(L_2)_2](NO_3)$ (**2**) have been synthesized by condensing substituted thiosemicarbazides like 4-methyl-3-thiosemicarbazide or 4-ethyl-3-thiosemicarbazide with 2-acetylpyridine. Both the metal complexes **1** and **2** are characterized by different spectroscopic techniques like IR, UV-Vis, ESR spectroscopy followed by elemental analysis, cyclic voltammetric measurement and single crystal X-ray structure analysis. X-ray crystal structures of complex **1** and **2** reveal that complex **1** is polymeric while complex **2** is dimeric in nature. The coordination geometry around Cu(II) are square pyramidal in which thiosemicarbazone Schiff base ligand coordinate to the central Cu(II) atom in tridentate fashion. The prominent interaction patterns of **1** and **2** with CT-DNA were examined by employing electronic absorption and emission spectral titrations, cyclic voltammetry and viscosity measurements. All the results show that CT-DNA binds with both copper (II) complexes **1** and **2**. Further, protein binding ability in vitro of complexes **1** and **2** with both BSA and HSA were carried out by multispectroscopic techniques and a static quenching pattern was observed in both cases. Molecular docking study was employed to ascertain the exact mechanism of action of **1** and **2** with DNA and protein molecules (BSA and HSA). In vitro cytotoxicity activity of complexes **1** and **2** towards AGS and A549 was evaluated by MTT assay which demonstrates that both complexes **1** and **2** have superior prospectus to act as anticancer agents.

Keywords: copper (II), complex, X-ray structure, cytotoxicity, molecular docking

Introduction

DNA is regarded as the primary target for the development of novel chemotherapeutic metal based drugs (Rambabu, Kumar, Tejaswi, Vamsikrishna, & Shivaraj, 2016; Lian et al., 2016; Kosiha, Parthiban, Ciattini, Chelazzi, & Elango, 2017; Chanphai, & Tajmir-Raihi, 2017). The main target for anticancer therapies is the development of high efficacy but low toxicity drugs (Rambabu, Kumar, Tejaswi, Vamsikrishna, & Shivaraj, 2016; Lian et al., 2016]. Generally cis-platin and its analogues are considered as most effective inorganic drugs for treatment of cancer (Kathiresan, Mugesh, Murugan, & Annaraj, 2017; Jaividhya, Ganeshpandian, Dhivya, Akbarsha, & Palaniandavar, 2015). But as a matter of fact, platinum based agents are not widely used due to their severe toxic side effect as well as for drug resistance (Lian et al., 2016). In this respect, recent research focuses on the design of metal-based anti-cancer agents with high level of selectivity but low toxicity (Kumar, Subarkhan, & Ramesh, 2015; Patra, Paul, Sepay, Kundu, & Ghosh, 2017). Among different transition elements, copper complexes are regarded as promising candidates that can substitute platinum drugs due to various possible stereochemistry, better solubility and also they will have greater affinity towards nucleic acid bases (Biswas et al., 2017; Lu et. al., 2014; Chen et al., 2007; Patra et al., 2013; Tabassum, Asim, Arjmand, Afzal, & Bagchi, 2012; Yilmaz et al., 2017; Suntharalingam et. al., 2012; Grau et al., 2015; Vafazadeh, Namazian, Chavoshiyan, Willis, & Carr, 2017). Copper is an essential trace element which is involved in normal functionalities of cells. Copper (II) complexes are generally found to be effective antimicrobials and also antitumor drugs (Kathiresan, Mugesh, Murugan, & Annaraj, 2017) All these facts clearly indicate that copper (II) complexes can be accepted as a promising alternative for platinum based drugs. Already many copper(II) Schiff base complexes have been evaluated for their more effective anticancer drugs [Lian et al., 2016; Tai, Lien, Lai, &

Khwaja, 1984; Wang, Keck, Lien, & Lai, 1990; Ganguly, Chakraborty, Banerjee, & Choudhuri, 2014; Ghosh et al., 2012; Ganguly et al., 2011).

Thiosemicarbazones are regarded as a class of Schiff base that essentially contain a thiourea part (Biswas et al., 2017; Haribabu et al., 2015; Guo, & Sadler, 1999; Dyson, & Sava, 2006; Orvig, & Abrams, 1999). The main interesting fact of this ligand is the combined hard (N-centre) as well as soft donor (S-centre) present in one ligand (Biswas et al., 2017). The biological potential of thiosemicarbazone is essentially dependent on the coordination to a metal ion by sulphur and nitrogen donor sites. Chelating ability of the ligand to the central metal ion and property of bridging ligands, etc ultimately establish the nuclearity of the final complex (Biswas et al., 2017; Lobana, Bawa, Hundal, & Zeller, 2008; Lobana, Bawa, Castineiras, Butcher, & Zeller, 2008; Lobana et al., 2006; Lobana et al., 2009; Lobana, Kumari, & Butcher, 2008; Ainscough, Brodie, Ranford, Waters, & Murray, 1992; Garcia-Tojal et. al., 1994; Bell, & Theochars, 1987; Bingham, Bogge, Muller, Ainscough, & Brodie, 1987; Garcia-Tojal et al., 1999; Ainscough, Brodie, Ranford, & Waters, 1997; Garcia-Tojal et al., 1996; Ainscough, Brodie, Ranford, & Waters, 1991; Singh, & Singh, 2001). Ligand architechture, oxidation state of metal ion and coordination geometry of the metal complex directly influence in its anticancer property (Kathiresan, Mugesh, Murugan, & Annaraj, 2017). Still now, almost all the studies of these types of ligand systems involved mono or dinuclear complexes with thiosemicarbazone Schiff bases (Brissos et. al., 2013; Giannicchi et al., 2013). In our earlier work, we synthesized one dinuclear thiosemicarbazone metal complex involving azide as bridging ligand (Biswas et al., 2017).

Bovine serum albumins (BSA) can be regarded as the most studied protein (Nanjundan et al., 2017; Singh, Pagariya, Jain, Naik, & Kishore, N. 2017; Zhou et al., 2018). BSA is basically the structural analogue of HSA. Significant interactions between many biologically active molecules and drugs with HSA have already been widely studied (Jafari et al., 2017). Serum

proteins generally plays essential role for the transport and metabolism of external drug (Biswas et al., 2017; Najjar, & Espósito, 2002; Salci, & Toprak, 2015). So for the study of binding property and the role of transport of copper based metal complexes, study of their interaction with DNA and serum proteins are essential (Nanjundan et al., 2017; Kosiha, Parthiban, Ciattini, Chelazzi, & Elango, 2017). BSA is now a days regarded as the mostly studied albumin as it is identical with HSA. Based on the above discussion, we introduced two substituted thiosemicarbazone ligands for the synthesis of copper (II) complexes **1** and **2**. Here, we synthesized two Schiff base ligands derived from 2-acetylpyridine and 4-methyl or 4-ethyl-3-thiosemicarbazides (Scheme 1) and their corresponding thiocyanato-bridged metal complexes $\{[Cu(L_1)(\mu\text{-}SCN)]_n(NO_3)_2$ (**1**) and $[Cu_2(\mu\text{-}SCN)(SCN)(L_2)_2](NO_3)$ (**2**)} respectively. We deliberately choose substituted thiosemicarbazide to increase bulkiness of the Schiff base ligand. Most of the thiosemicarbazide metal complexes devoid of any bridging but here we introduced bridging thiocyanate for both the complexes **1** and **2**. Both the complexes **1** and **2** are characterized by elemental analyses, FT-IR, UV-Vis, ESR spectroscopy, cyclic voltammetry and single crystal X-ray structure analysis. In-vitro DNA binding experiments of copper (II) substituted thiosemicarbazone complexes **1** and **2** signifies that these complexes are effective DNA binding agents and can act as potent chemotherapeutics. The protein binding studies were examined using serum albumins by multispectroscopic techniques. Both BSA and HSA were taken for the purpose of analysis due their similar structural homology and both the complexes **1** and **2** shows significant protein interactions. The molecular interaction of synthesized complexes **1** and **2** with both DNA and protein molecules are confirmed by molecular docking study to ascertain the ligand conformation and also their orientations in the binding site of the receptor. Finally, the in-vitro cytotoxicity of complexes **1** and **2** was investigated on two different human cancer cell lines (AGS and A549) which demonstrates that both **1** and **2** have significant broad-spectrum

anticancer activity with IC_{50} values 11.098 µM for AGS and 2.20 µM for A549 for **1** and 2.34 µM for both AGS and A549 in case of **2** respectively which are very close to the IC_{50} values of cis-platin for both AGS and A549 cell lines.

Experimental Section

Materials

All the chemicals and reagents were purchased from commercial sources and were used without further purification. 4-methyl-3-thiosemicarbazide, 4-ethyl-3-thiosemicarbazide, 2-acetylpyridine, bovine serum albumin (BSA), human serum albumin (HSA) and tetrabutylammonium perchlorate (TBAP) were purchased from Sigma-Aldrich. Copper (II) nitrate, ammonium thiocyanate (NH_4SCN) were purchased from E-Marck. Calf-thymus DNA (CT-DNA) and Tris-HCl buffer were obtained from SRL and Ethidium bromide (EB) was from Spectrochem.

Physical measurements

Fourier Transform Infrared spectra (4000-400 cm^{-1}) of the complexes **1** and **2** were recorded on a Perkin-Elmer SPECTRUM - 2 FT-IR spectrophotometer in solid KBr matrices. Electronic spectra of the titled complexes were recorded at 300K on a Perkin-Elmer Lambda-35 UV-vis spectrophotometer in Tris-HCl buffer medium. Elemental analyses were carried out with a Perkin-Elmer 2400 II elemental analyzer. Emission data were collected on a Perkin-Elmer LS 55 fluorescence spectrophotometer at 300K in Tris-HCl buffer solution. For all luminescence measurements, an excitation and emission slit width of 10 nm was used. All the electrochemical experiments were carried out with three electrode configuration using a CH 660E cyclic voltammeter in Tris-HCl buffer medium. Saturated calomel electrode (SCE)

as reference, Pt wire-electrode as counter electrode and glassy carbon electrode as a working electrode were used as three electrode system with tetrabutylammonium perchlorate (TBAP) as a supporting electrolyte at a scan rate of 50 mV sec^{-1}. All the electrochemical data were recorded under dry nitrogen environment. Nitrogen gas was passed into the sample solution at a constant rate for 1 minute. The viscosity measurements were carried out using a semi-micro viscometer at 27°C.

Synthesis of Schiff base ligands and copper complexes

Synthesis of Schiff Base ligand (HL_1)

A methanolic solution of 4-methyl-3-thiosemicarbazide (5 mmol, 0.526 g) and a methanolic solution 2-acetylpyridine (5 mmol, 0.561 ml) were mixed and refluxed for 2 hours (shown in Scheme 1). After that, the solution became colourless. The colourless reaction mixture was then cooled at room temperature and it was used without further purification.

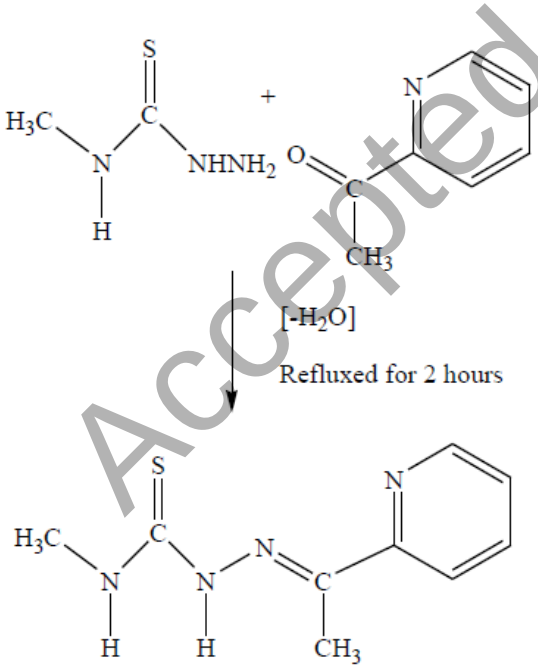

(HL_1)

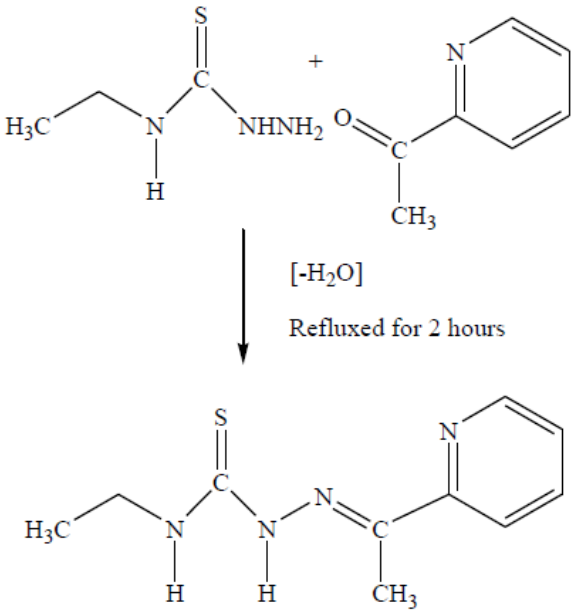

(HL_2)

Scheme 1. Formation of Schiff base ligands (**HL_1**) and (**HL_2**).

Synthesis of Schiff base ligand (HL_2)

Schiff base ligand **2** was prepared following the same procedure as in **1**, using 4-ethyl-3-thiosemicarbazide (5mmol, 0.596 g) instead of 4-methyl-3-thiosemicarbazide (shown in Scheme 1).

Synthesis of complex $[Cu(L_1)(\mu\text{-}SCN)]_n(NO_3)_2$ (1)

A methanolic solution of copper (II) nitrate trihydrate (0.2416 g, 1mmol) was mixed to a methanolic solution of Schiff base ligand **1** (1 mmol) followed by constant stirring. Then the reaction mixture becomes light green. After that, 1 mmol methanolic solution of ammonium thiocyanate (0.076 g) was added dropwise to the resultant light green solution with stirring. After addition, the solution turned deep green and the reaction mixture was refluxed for 2 hours. Then the solution was filtered and left for crystallization. After a weak, dark green coloured single crystals were appeared and it was used for characterization.

Yield: 68% (0.278 g).

Anal. Calc. for [C_{22} H_{20} Cu_2 N_{12} O_7 S_4]: C, 32.20; H, 2.44; N, 20.49%. Found: C, 32.14; H, 2.40; N, 20.44%.

IR (KBr, cm^{-1}): 3439(s), 1513(s), 2083(s), 823(m), 783 (s) and 497(s).

Synthesis of complex $[Cu_2(\mu\text{-}SCN)(SCN)(L_2)_2](NO_3)$ (2)

Complex **2** was prepared following the same procedure as in **1**, using Schiff base **2** instead of Schiff base **1**.

Yield: 66% (0.256 g).

Anal. Calc. for [C_{22} H_{24} Cu_2 N_{11} O_3 S_4]: C, 35.39; H, 3.22; N, 20.65%. Found: C, 35.35; H, 3.20; N, 20.62%.

IR (KBr, cm^{-1}): 3435(b), 1590(s), 2080(s), 821(m), 775 (m) and 474(m).

X-Ray crystallography

Good quality single crystals of **1** and **2** were mounted on a SuperNova, Dual, Cu at zero, Eos diffractometer, equipped with graphite monochromatized Cu Kα radiation (λ = 1.54178 Å) fine-focus sealed tubes. Intensity data were collected at 298(2) and 100(2) K respectively using ω scans. Crystal data were collected using a CrysAlisPro, Agilent Technologies,Version 1.171.37.33c. Data refinement and reduction were performed using CrysAlisPro, Agilent Technologies,Version 1.171.37.33c software. Multiscan absorption corrections were applied empirically to the intensity values (*T*min = 0.511 and *T*max = 0.572 for **1** and *T*min = 0.562 and *T*max = 0.654 for **2** respectively) using SADABS, Bruker-2008. (Bruker 2000, SADABS, SMART and SAINT. Bruker AXS Inc., Madison, isconsin,USA, 2008). The structures were solved by direct methods, and refined with full-matrix least-squares based on *F2* using program using the program SHELXS-97 (Sheldrick, 2008). All non-hydrogen atoms were refined anisotropically. C-bound hydrogen atoms were placed geometrically and refined using a riding model approximation. The molecular graphics and crystallographic illustrations for **1** and **2** were prepared using Bruker SHELXTL and ORTEP programs.

DNA-copper complexes interaction study

Electronic absorption spectrophotometric study

Using DMSO solutions of complexes **1** and **2** and dilution were made using Tris-HCl buffer. Binding efficiency of substituted thiosemicarbazone copper (II) complexes **1** and **2** with CT-DNA were studied using UV-Vis titration. A stock solution of CT-DNA was prepared and stored at 4°C and used within 4 days. The CT-DNA concentration was measured from its absorption intensity at 260 nm using a molar absorption coefficient value of 6600 dm^3mol^{-1} cm^{-1} (Mandegani, Asadi, Karbalaei-Heidari, Rastegari, & Asadi, 2016; Reichmann, Rice, Thomas, & Doty, 1954). Ratio of peaks at 260 and 280 nm (A_{260}/A_{280}) was found to be 1.9 which shows DNA was sufficiently free of proteins (Muralisankar, Sujith, Bhuvanesh, & Sreekanth, 2016). Electronic absorption spectral titrations were carried out by keeping a fixed concentration of the metal complexes (50µM) and varying the CT-DNA concentration (0-140 µM). Absorption spectra for each case were studied after 10 min.

Competitive binding experiments

The competitive binding interaction study of each of the complexes **1** and **2** with EB were investigated using fluorescence spectral method to study if the complexes **1** and **2** are able to displace EB from its DNA-EB complex. Ethidium bromide is a classical intercalator whose fluorescence intensity is enhanced upon complexation with DNA (Biswas et al., 2017; Ingle et al., 2015; Manikandan, Chitrapriya, Jang, & Viswanathamurth, 2013). The experiments were carried out by adding an incremental increasing amount of a solution of complexes **1** and **2** ([complex] = 0-60 µM) successively into the EB-DNA solution ([DNA] = 20 µM, [EB] = 10 µM). Emission spectra of **1** and **2** were obtained at room temperature in the region between 525 and 750 nm with a fixed excitation wavelength of 510 nm. For every addition,

the samples were equilibrated for 10 mins before the fluorescence emission spectra were recorded.

Electrochemical studies

To determine the redox property of complexes **1** and **2**, cyclic voltammetry were carried out using a CH660E Electrochemical work station with three electrode cell comprising of a saturated calomel electrode (SCE) as reference, Pt wire-electrode as counter electrode and glassy carbon electrode as a working electrode, using TBAP as supporting electrolyte (100 µM). Cyclic voltammograms of complexes **1** and **2** were recorded in Tris-HCl buffer medium at a scan rate of 50 mV sec^{-1}. All experiments were performed using fixed concentration of copper (II) complexes **1** and **2** and in absence and in presence of varying amount of CT-DNA.

Viscosity measurements

Viscosity experiments were investigated with the help of a semi-micro viscometer which is immersed in a thermostatic water bath at room temperature. Lengthening of the DNA helix was studied in absence and in presence of increasing amounts of complexes **1** and **2** respectively. The concentration of CT-DNA was fixed at 100 µM and flow time of the same was measured in absence and in presence of the complexes **1** and **2** respectively. Data for each sample was measured thrice and the average flow time was taken. Relative viscosities for CT-DNA were calculated from the relation $\eta = (t-t_0)/ t_0$, where t is the observed flow time of DNA containing complexes **1** or **2** and t_0 is the flow time of Tris-HCl buffer itself (Manikandan, Chitrapriya, Jang, & Viswanathamurth, 2013). $(\eta/\eta_0)^{1/3}$ *versus* binding ratio [complex]/[DNA] were plotted where η is the viscosity of CT-DNA in the presence of complexes **1** or **2** and η_0 is the viscosity of CT-DNA alone in Tris-HCl buffer.

Protein binding studies

Protein binding experiments were studied using absorbance and fluorescence measurements. Fluorescence spectra of **1** and **2** were recorded from 200 to 500 nm for both BSA and HSA with the excitation wavelength 279 nm. For all DNA binding experiments, Tris-HCl buffer were used. Stock solutions of BSA and HSA were prepared in 40 µM Tris-HCl buffer (pH = 7.2) and stored in the dark at 4°C. 2.5 ml of protein stock solutions (40 µM) were titrated by gradual addition of 5 µM of stock solutions of complexes **1** and **2** (0-70 µM). Similar experiments were performed by using UV-Vis titration method also.

Cytotoxicity study

Chemicals

Annexin V-assay Kit was purchased from (eBioscience). Anti-mouse antibodies against Bax, Bcl2, PCNA, GAPDH and anti-rabbit antibodies against P53, Caspase3 were procured from Santa Cruz (USA), bacitracin, leupeptin, pepstatin A, PMSF, phosphatase inhibitor cocktails. A-Sepharose beads, RNase, NAC and NBT were purchased from Sigma (St. Louis, MO). Nitrocellulose membrane, and filter papers were obtained from Pall Corporation, USA.

Cell lines and culture

Human lung (A549) and gastric (AGS) cancer cell lines were obtained from NCCS Pune. Cells were cultured at 37 °C in humidified atmosphere of 5% CO_2–95% air. Cell culture medium contains DMEM and F12K (Gibco, invitrogen, USA) supplemented with 10% heat inactivated fetal bovine serum (FBS; Invitrogen.) and 1% penicillin G and streptomycin (Life Technologies, Rockville, MD, USA). The cells, initially seeded at the concentration of 10^4cells/mm^2, were incubated at 37°C with humidity saturated controlled atmosphere and 5% CO_2.

Hemolytic assay

Fresh human blood was centrifuged at 4000 × g for 10 min and the cell pellet was washed thrice and re-suspended in 10mM PBS at pH 7.4 to obtain a final concentration of 1.6×10^9 erythrocytes/ml. Equal volumes of erythrocytes were incubated with varying concentrations of **1** and **2** with shaking at 37ºC for 1hr. Samples were then subjected to centrifugation at 3500 × g for 10 min at 4ºC. RBC lysis was measured at different drug concentrations by taking absorbance at an OD of 540 nm. Complete hemolysis (100%) was determined using 1% Triton X 100 as a control. Hemolytic activity of the spice active components was calculated in percentage using the following Equation:

$H=100 \times (Op-Ob)/(Om-Ob)$

where, Op is the optical density of given drug concentration, Ob is the optical density of buffer and Om is the optical density of Triton X 100.

Cell viability Assay on PBMC

The Trypan Blue dye exclusion test is used to determine the number of viable cells present in a cell suspension. It is based on the principle that live cells possess intact cell membranes that exclude trypan blue, whereas dead cells do not. The effect of complexes **1** and **2** on the viability of PBMC cells was determined by Trypan blue exclusion test. Cells were treated with varying of these molecules and at definite time point (24 hrs) the cells that could exclude the Trypan blue dye were counted in haemocytometer as viable cells.

MTT assay

This colorimetric assay is based on the activity of mitochondrial succinate dehydrogenase enzyme in live cells to reduce the yellow water soluble substrate MTT into an insoluble, colored formazan product which is measured spectrophotometrically at 595 nm. Since reduction of MTT can only occur in metabolically active cells, the level of activity is a measure of the viability of cells. The cytotoxicity of these synthetic molecules was tested on AGS and A549 cells by MTT-assay. Briefly, 2×10^4cells were seeded in a 96-well microtitre plates and incubated with different concentrations of these synthetic molecules. After 12hr of exposure to these molecules, 10 µl of MTT (5mg/mL) was added to each well, and the cells were incubated in dark at 37°C for an additional 4 h. Thereafter, the medium was removed, the formazan crystals were dissolved in 100 µL of dissolving solution (10% SDS in isopropanol), and the absorbance measured at 595 nm wavelength.

Cell cycle distribution analysis

Cell cycle analysis is a method in that employs flow cytometry to distinguish cells in different phases of the cell cycle based on fluorescence intensity of the stained cells at certain wavelength. For the determination of cell cycle phase distribution of nuclear DNA, in vitroAGS, A549 cells (1×10^6 cells) were harvested. After making a single cell suspension, cells were fixed with 3% p-formaldehyde, permeabilized with 0.5% Triton X-100, and nuclear DNA was labeled with propidium iodide (PI, 125µg/mL) after RNase (40µg/ml) treatment. Cell cycle phase distribution of nuclear DNA was determined on FACS Caliber using Cell Quest Software (Becton-Dickinson Histogram display of DNA content (x-axis, PI fluorescence) versus counts (y-axis) has been displayed.

Annexin V assay

Apoptosis assays were carried out based on the instruction from the Annexin V Apoptosis Kit (eBioscience). Briefly, PI and Annexin V were added directly to AGS and A549 cells treated with complexes **1** and 2 (0.5µg/ml). The mixture was incubated for 15 min at 37ºC. Cells were fixed and then analysed on FACS VERSE (equipped with 488 nm Argon laser light source; 515 nm band pass filter, FL1-H, and 623 nm band pass filter, FL2-H) (Becton Dickinson). Electronic compensation of the instrument was done to exclude overlapping of the emission spectra. Total 10,000 events were acquired, the cells were properly gated and dual parameter dot plot of FL1-H (x-axis; Fluos-fluorescence) versus FL2-H (y-axis; PI-fluorescence) shown in logarithmic fluorescence intensity.

Western blot analysis

Western blot (also called protein immunoblotting, because an antibody is used to specifically detect its antigen) is a widely accepted analytical technique used to detect specific proteins in the given sample. By analyzing location and intensity of the band formed, expression details of the target proteins in the given cells could be obtained. AGS and A549 cell lysates were obtained and equal amounts of protein from each sample were diluted with loading buffer, denatured, and separated by 10% sodium dodecyl sulfate-polyacrylamide gel electrophoresis (SDS-PAGE) followed by protein transfer to nitrocellulose membrane. The effect of complexes **1** and **2** on GAPDH, PCNA, Bax, Bcl-2, p53 and active caspase3 expressions were checked on AGS and A549 cancer cells. The blot was incubated with respective primary antibody (anti-PCNA, anti-Bax, anti-Bcl2, anti-p53 and anti-active caspase3 antibody) followed by blotting with HRP-conjugated secondary antibody. The blots were then detected by using a chemiluminescent kit from Santacruz Biotechnology (USA). This analysis was performed two times.

Statistical analysis

The experiments were repeated three times and the data were analyzed statistically. Values have been represented as mean ± sd. Data were analyzed and Student's t-test was used to evaluate the statistical differences. Statistical significance was considered when $P < 0.05$.

***In silico* binding mode analysis of complexes 1 and 2 with the macromolecules (HSA, BSA and duplex DNA) by molecular docking study**

The x-ray crystal structures of HSA (PDB ID: 4IW2), BSA (PDB ID: 4F5S), and duplex DNA d(CGATCG)2 hexamer (PDB ID: 1Z3F) were obtained from Protein Data Bank (PDB). All water molecules and ions were removed, and hydrogen atoms were added to the functional groups with the appropriate geometry within the macromolecules. All the macromolecules (HSA, BSA and duplex DNA) and complexes **1** and **2** were typed with CHARMm forcefield (Feller, & Mackerell, 2000; Mackerell et al., 1998) before analyzing docking studies. The possible binding sites on the receptor were identified using based on the shape of the receptor molecule. The possible conformations of complexes **1** and **2** poses were generated using CDOCKER program (Wu, Robertson, Brooks III, & M. Vieth, 2003). The receptor is held rigid while the complexes **1** and **2** are allowed to flex during the refinement. The molecular docking poses of each synthesized molecules were ranked according to CDOCKER interaction energy. Calculations of the binding energy were carried out to select the most suitable pose of the each molecule. Finally energy minimization of the docked receptor-complex was performed for further analysis. All procedures were carried out using Discovery Studio software (Accelrys Discovery Studio Visualiser v 3.5.0.12158, Accelrys Software Inc, San Diego).

Results and discussion

The Schiff base ligands (**HL_1** and **HL_2**) were prepared by the condensation reaction between 2-acetylpyridine and 4-methyl-3-thiosemicarbazide or 4-ethyl-3-thiosemicarbazide respectively in methanol medium. Complexes **1** and **2** were synthesized by the reaction of copper(II) nitrate with the Schiff base ligands **HL_1** and **HL_2** and ammonium thiocyanate in same solvent. Both the complexes were characterized by various spectroscopic techniques like FT-IR, UV-Vis and ESR spectroscopy along with by structural, analytical methods and cyclic voltammetric techniques.

Infrared spectral study

The IR-spectra of copper (II) complexes **1** and **2** are shown in the Figure S1. The infrared spectra of complex **1** and **2** show IR peaks at 1513 and 1590 cm^{-1} respectively for γ(C=N) stretching frequency. The above observation confirmed the coordination of the azomethine nitrogen to the metal ion. Peaks at 783 and 775 cm^{-1} for **1** and **2** respectively appeared for γ(C-S) (Kalaivani et al., 2014: Prabhakaran et al., 2008). Peaks appeared at 497 and 473 cm^{-1} respectively for **1** and **2** are due to the formation of Cu–N bonds. Peaks at 823 and 821 cm-1 for complexes **1** and **2** respectively show sulphur coordination to copper (II) centre. Both the complexes **1** and **2** show sharp peaks at 2083 and 2080 cm^{-1} respectively for γ(SCN) bridging. The spectra of complexes **1** and **2** also displayed characteristic absorption band at 3439 and 3435 cm^{-1} respectively due to γ(N-H) vibration.

Electronic spectral study

Electronic absorption spectra of complexes **1** and **2** show three characteristic absorption bands (Fig. S2). The UV-Vis spectra of both **1** and **2** are very similar. Both **1** and **2** show a

low energy field (LF) band at 610 and 611 nm respectively and two high energy ligand-based bands in the region 303-304 nm and 408-409 nm respectively. The bands at 408 and 409 nm of the complexes **1** and **2** respectively are due to ligand to metal charge transfer (LMCT) transition (Chew, Lo, Sinniah, Sim, & Tan, 2014; Krishnamoorthy, Sathyadevi, Cowley, Butorac, & Dharmaraj, 2011; Sreeja, Kurup, Kishore, & Jasmin, 2004; Sathyadevi et al., 2012). The intraligand **π→π*** transition of the coordinated imines are observed at 303 and 304 nm respectively. The low intensity bands at 610 and 611 nm for **1** and **2** may be correlated to **d→d** transition. The electronic absorption spectra of complexes **1** and **2** were carried out for three successive days maintaining the same concentration and same solvent but there were no distinct changes. This observation clearly indicates that both the complexes **1** and **2** are stable in the condition of analysis.

Cyclic voltammetric study

Electrochemical study was carried out for complexes **1** and **2** in Tris-HCl buffer medium under nitrogen atmosphere in the potential range from +2.0 to -2.0 V using tetrabutylammonium perchlorate as supporting electrolyte. The voltammograms of complexes **1** and **2** are shown in Figure S3. Both the copper (II) complexes **1** and **2** show one prominent oxidative peak at +1.05 and +0.92 V respectively which corresponds to Cu(II) to Cu(III) oxidation. Figure S3 show reduction peaks of both the Cu (II) complexes **1** and **2** with cathodic wave potential -0.88 and -0.69 V respectively corresponding to the Cu(II) to Cu(I) redox couple.

X-ray crystal structure description

Structural description of complex 1

Single crystal X-ray analysis reveals that complex **1** crystallizes in space group *P*nma *(No. 33)* of orthorhombic crystal system. A structural view of complex **1** with atom numbering scheme is shown in Figure 1.

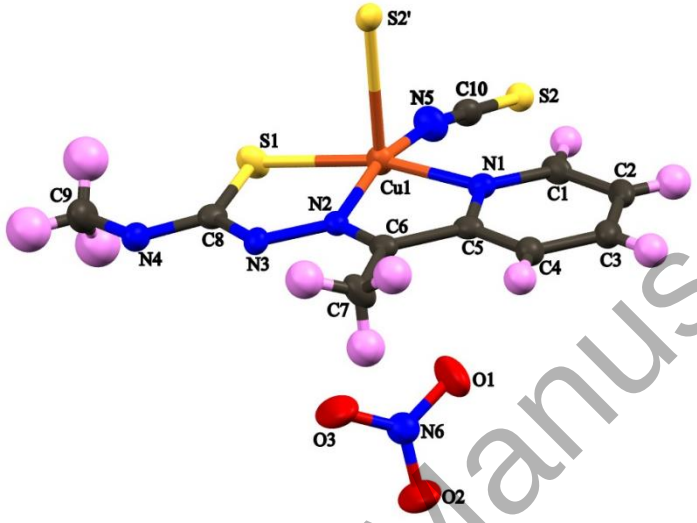

Figure 1. ORTEP view of complex **1** with displacement ellipsoids drawn at 50% probability level (Hydrogen atoms are omitted for clarity)

Table 1. Crystallographic data and structural refinement of complexes **1** and **2.**

	1	**2**
empirical formula	$C_{22}H_{20}Cu_2N_{12}O_7S_4$	$C_{22}H_{24}Cu_2N_{11}O_3S_4$
formula weight ($g\ mol^{-1}$)	819.88	745.90
temperature	298	100
crystal system	Orthorhombic	Triclinic
space group	*P*nma	*P*-1
a (Å)	16.5584(7)	8.8167(3)
b (Å)	24.2286(12)	13.4992(6)
c (Å)	7.8056(3)	14.0175(6)
α (deg)	90	110.347(4)
β (deg)	90	95.359(3)
γ (deg)	90	106.419(3)
V(Å^3)	3131.5(2)	1465.98(12)
Z	2	4
dcalc (g cm^{-3})	1.739	1.690
μ (mm^{-1})	4.728	4.861
F(000)	1656	758
crystal size (mm^3)	0.22 × 0.13 × 0.12	0.13 × 0.12 × 0.09
θ range (deg)	5.34 - 66.51	3.44 - 66.28
measured reflections	2802	5105
independent reflections	2671	4612
R(int)	0.0401	0.0362
goodness-of-fit on F^2	1.096	1.097
final *R* indices [I > 2σ(I)]	*R*1=0.0774, *wR2*= 0.1824	*R*1=0.0445, *wR2*=0.1173
R indices (all data)	*R*1=0.0803, *wR2*= 0.1839	*R*1 = 0.0803, *wR2*=0.1217
$\Delta\rho$min and $\Delta\rho$max	-1.296 and 1.302 (e Å^{-3})	-1.015 and 0.855 (e Å^{-3})

Crystallographic data and structural refinement of complex **1** and selected bond lengths and bond angles are summarized in Table 1 and 2 respectively. The asymmetric units contain one tridentate ligand moiety, two thiocyanato anions coordinating the central copper(II) atom via S-end and N-end respectively and a nitrate anion in lattice. Partial packing diagram (Fig. 2) shows that the complex contains one central Cu atom, which acquires a square pyramidal geometry with the ligand (bonded with NNS donor set) and two thiocyanato anion, which were connected to the metal atom through their nitrogen and sulphur atom namely N1, N2 and S1 from the ligand and N5 and S2 from the thiocyanato anion. The S2 atom from the thiocyanato anion is at the peak of pyramid where the basal plane is bonded to the donor

atoms (N1, N2 and S1) from the ligand along with N-end (N5) of another thiocyanato anion i.e., three nitrogens and a sulphur atom. The square pyramid thus formed is slightly distorted in nature and the Addison parameter τ is 0.029. The same thiocyanato anion which donates N5 to the central metal atom is also coordinated to another metal centre with its S-end, namely S2. So here, the thiocyanato anion performs as a bridging ligand with an *end-on* bridging mode. The donor atoms N1 and N2 form a five member ring N1C5C6N2Cu1 and S1 and N2 also form a five member ring S1C8N3N2Cu1 with the central metal atom respectively. The angles subtended the Cu1 atom ranges from 80.0(2)° to 165.7(3)°.

Table 2. Selected bond lengths (Å) and bond angles (^{0}) for complex **1**.

Complex **1**	
Cu1-S1	2.2773(19)
Cu1-S2	2.7673(19)
Cu1-N1	2.021(5)
Cu1-N2	1.965(5)
Cu1-N5	1.943(7)
S1-Cu1-S2	97.43(6)
S1-Cu1-N1	164.01(15)
S1-Cu1-N2	85.21(15)
S1-Cu1-N5	96.2(2)
S2-Cu1-N1	89.61(15)
S2-Cu1-N2	93.36(15)
S2-Cu1-N5	100.6(2)
N1-Cu1-N2	80.0(2)
N1-Cu1-N5	96.6(2)
N2-Cu1-N5	165.7(3)

The relative deviations of bond angles and lengths from the ideal values (Table 2) also support the distorted square pyramidal geometry of the Cu(II) centre. The bond lengths of Cu-N are within range 1.943(7)- 2.021(5) Å and the Cu-S bond lengths are within range of 2.2773(19)- 2.7673(19) Å.

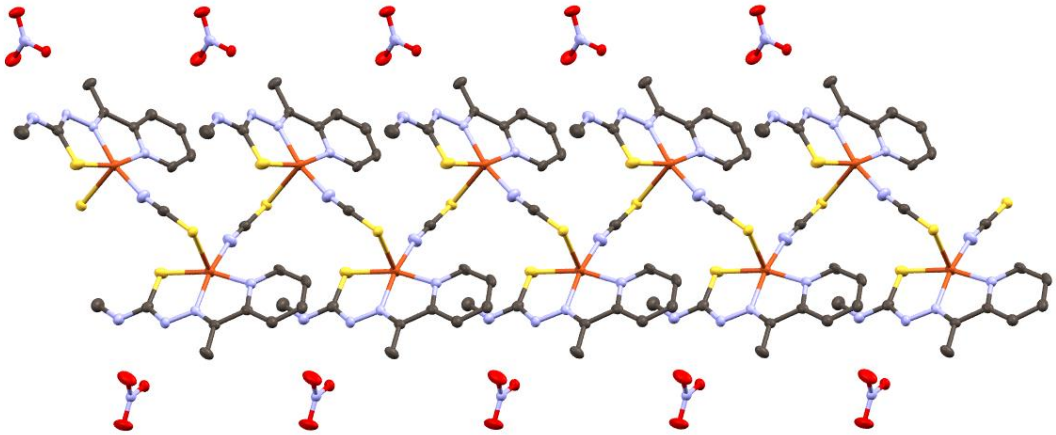

Figure 2. Packing diagram of complex **1**

An elaborate view of the structure shows that the *end-on* bridging mode of the thiocyanate anion leads to formation of a 1D chain polymer (Fig. 2), actually the thiocyanato anion satisfies both primary and secondary valency of the central copper atom. The +2 charge on the copper atom is satisfied by two thiocyanato anion which has a contribution of -1/2 and -1 from the lattice nitrate anion. The nitrate ion also has no contribution in the structure rather than some non-classical hydrogen bonding.

There are two types of intramolecular non-classical hydrogen bond in the complex. They are C-H···S hydrogen bond where the hydrogen bond donor is the aromatic ring of the pyridine moiety and the acceptor is the thiocyanato ion [C2-H2···S2, (x,y,1+z) 3.745(7)] and C-H···O, where the donor is methyl group and the acceptor is nitrate ion [C7-H7A···O4, (x,1/2-y,z) 3.470(9)].

Structural description of complex 2

Single crystal X-ray analysis reveals that complex **2** crystallizes in space group *P*-1 of triclinic crystal system. A structural view of complex **2** with atom numbering scheme is shown in Figure 3.

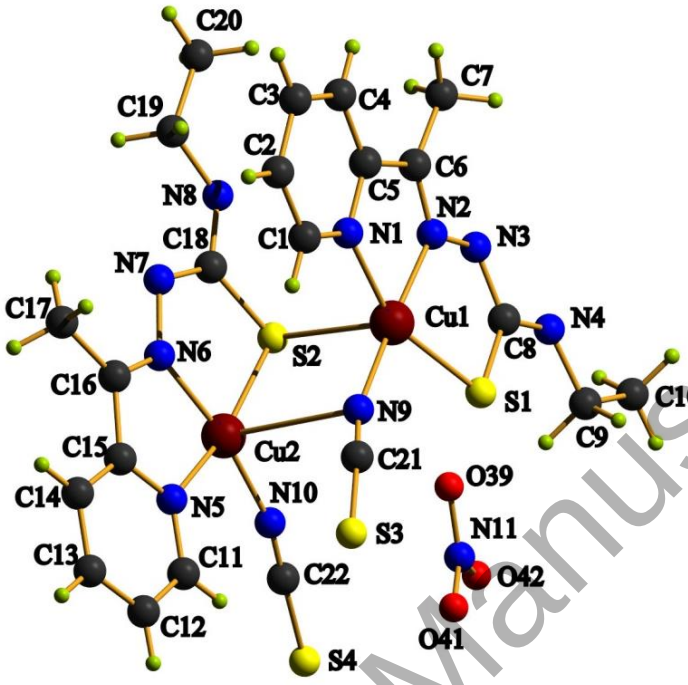

Figure 3. ORTEP view of complex **1** with displacement ellipsoids drawn at 50% probability level (Hydrogen atoms are omitted for clarity)

Crystallographic data and structural refinement of complex **2** and selected bond lengths and bond angles are summarized in Table 1 and 3 respectively.

Table 3. Selected bond lengths (Å) and bond angles (^{0}) for complex **2**.

Complex **2**	
Cu1-S1	2.3052(10)
Cu1-S2	2.6966(10)
Cu1-N1	2.033(3)
Cu1-N2	1.971(3)
Cu1-N9	2.012(3)
Cu2-S2	2.2680(10)
Cu2-N5	2.008(4)
Cu2-N6	1.956(3)
Cu2-N9	2.916(3)
Cu2-N10	1.944(4)
S1-Cu1-S2	97.22(3)
S1-Cu1-N1	158.25(8)
S1-Cu1-N2	84.12(8)
S1-Cu1-N9	96.94(8)
S2-Cu1-N1	96.69(8)
S2-Cu1-N2	96.69(8)
S2-Cu1-N9	95.10(8)
N1-Cu1-N2	79.02(11)
N1-Cu1-N9	98.40(11)
N2-Cu1-N9	173.74(11)
S2-Cu2-N5	164.68(11)
S2-Cu2-N6	84.87(9)
S2-Cu2-N9	84.09(6)
S2-Cu2-N10	99.14(12)
N5-Cu2-N6	80.80(14)
N5-Cu2-N9	92.05(11)
N5-Cu2-N10	95.90(16)
N6-Cu2-N9	96.01(10)
N6-Cu2-N10	169.78(14)
N9-Cu2-N10	93.76(13)

The asymmetric unit of the complex **2** shows that the complex has a dimeric structure, which contains two electronically neutral tridentate ligand moieties, two thiocyanato anions coordinating each of the central copper atoms via N-end and a nitrate anion in lattice. Figure 3 shows that the dimeric complex contains two central Cu atoms namely Cu1 and Cu2, both of which acquire square pyramidal geometries with the ligands (bonded with NNS donor set) and the thiocyanato anions. The coordination environment of Cu1 consists of three nitrogen and two sulphur atoms namely N1, N2 and S1 from one of the ligand and S2 from the other

ligand of the asymmetric unit along with N9 from the thiocyanato anion. Whereas, the coordination environment of Cu2 is surrounded by four nitrogen atoms and a sulphur atom. Alike Cu1, the ligand donates three atoms (N5, N6 and S2) to Cu2 and the remaining coordination sites are filled with the thiocyanato anions. For Cu2, one of the thiocyanto anion is bonded to the metal atom with N10 atom i.e., act as a monodentate ligand and the other position is bonded to N9, which is from another thiocyanto anion. The later acts as an *end-to-end* bridging (i.e., bidentate) ligand, which connects Cu1 and Cu2. The peak of pyramid for Cu1 is occupied by S2 atom from one of the ligand and the basal plane is bonded to the donor atoms (N1, N2 and S1) from the ligand along with N-end (N9) of the bridging thiocyanato anion i.e., a total of three nitrogens and a sulphur atom. The square pyramid thus formed is highly distorted in nature. The apical position of the pyramid formed around Cu2 is occupied by N9 of the bridging thiocyanato anion and the basal plane is occupied by S2, N6, N5 from the ligand and N10 from the singly coordinated thiocyanato anion. The angles subtended the Cu1 atom ranges from 79.02(11)° to 173.74(11)° and that of Cu2 are ranging between 80.80(14)° to 169.78(14)°. The relative deviations of bond angles and lengths from the ideal values (Table 3) also support the distorted square pyramidal geometry of the Cu(II) centre. The fact, that the distortion of C4v symmetry towards *D*3h is somehow greater for Cu1 (Addison parameter: Cu1= 0.258, Cu2= 0.085) is very much noticeable in **2**. But, to be exact, the geometry around Cu2 acquires nearly a perfect square pyramidal one. The bond lengths of Cu1-N are within range 1.971(3)- 2.033(3) Å and the Cu-S bond lengths are within range of 2.3052(10)- 2.6966(10) while Cu2-N ranges from 1.944(4) to 2.916(3) Å. These are consistent with most mixed-valence Cu23+ complexes documented previously, (Lecloux, Davydov, & Lippard, 1998; Lo et al., 2000; Glaser, Lügger, & Fröhlich, 2004) in which two metal atoms have virtually identical coordination environments. From the above observation it can be concluded that **2** is a copper(1.5), copper(1.5) compound (Zhang et al., 2002). So the

+3 charge arises from copper atoms is satisfied by two thiocyanato anion which has a contribution of -1 each and -1 from the lattice nitrate anion. The nitrate ion has no contribution in the structure rather than some non-classical hydrogen bonding.

DNA binding studies

Electronic absorption titration

Before titration of complexes **1** and **2** with CT-DNA, its stability in the Tris-HCl buffer solution (pH ~7.2) at room temperature was observed by UV-Vis spectroscopy for 24 h. No distinguishable change was noticed under this condition. UV-Vis spectra of complexes **1** and **2** in DMSO, Tris-HCl buffer medium and acetonitrile were also compared and shown in Figure S4 (Supplementary information). No significant differences were noticed in the spectra taken in three different solvents [refer to Table T1 of Supplementary information]. All these data prove that complexes **1** and **2** were stable under the condition of experiments. [For a detailed discussion on the integrity of complexes **1** and **2** in aqueous medium, see Supplementary information].

DNA binding activities of metal complexes have been a clue of paramount importance for the development of effective metal complexes for the screening of metal based chemotherapeutic drugs (Chew, Lo, Sinniah, Sim, & Tan, 2014; Barve et al., 2009; Efhimiadou et al., 2007). Generally different kind of binding modes are observed when metal complexes bind with DNA e.g. non-covalent binding, intercalation etc (Muralisankar, Sujith, Bhuvanesh, & Sreekanth, 2016). Change in absorbance e.g. hypochromism and a bathochromic shift in wavelength is the characteristics of intercalative binding between DNA base pairs and aromatic chromophore of the test compounds (Sathyadevi, Krishnamoorthy, Butorac,

Cowley, & Dharmaraj, 2012). Strength of the intercalative binding interaction directly influences hypochromism (Mandegani, Asadi, Karbalaei-Heidari, Rastegari, & Asadi, 2016; Krishnamoorthy, Sathyadevi, Cowley, Butorac, & Dharmaraj, 2011; Saswati et al., 2015; Kumar, Gorai, Santra, Mondal, & Manna, 2012). When the investigating compounds intercalate to the base pairs of DNA, the π* orbital of the intercalators can couple with the π orbital of the base pairs, thereby decreases the $\boldsymbol{\pi \rightarrow \pi^*}$ transition probabilities which ultimately produce a hypochromism (Krishnamoorthy et al., 2012; Li, Yang, Wang, & Qin, 2008). When the extent of hyperchromism is observed in the absorption spectra of a test compound with increasing concentration of DNA, it signifies the non-intercalative interaction pattern between test compound and DNA molecules (Mistri, Puschmann, & Manna, 2016; Mancin, Scrimin, Tecilla, & Tonellato, 2005; Tjioe, Meininger, Joshi, Spiccia, & Graham, 2011). To identify the kind of interaction of copper (II) complexes **1** and **2** with DNA, 50 µM solution of complexes **1** or **2** were titrated with 10-140 µM CT-DNA in Tris-HCl buffer solution having pH 7.2 at room temperature (Fig. 4).

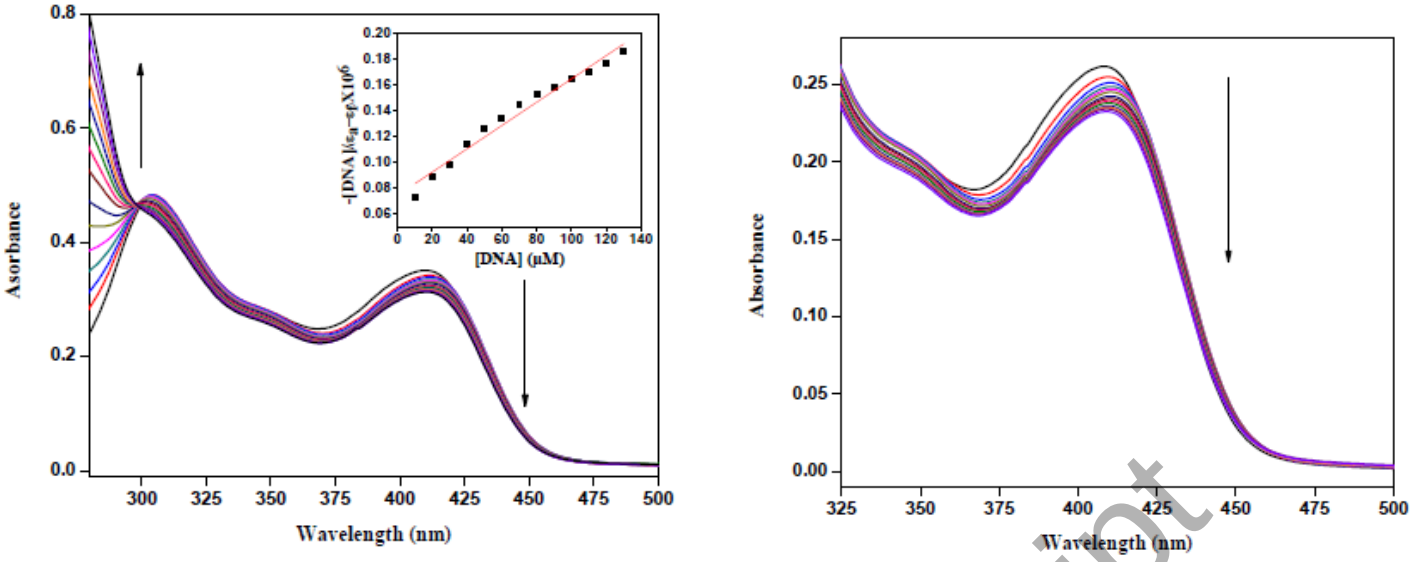

(A)

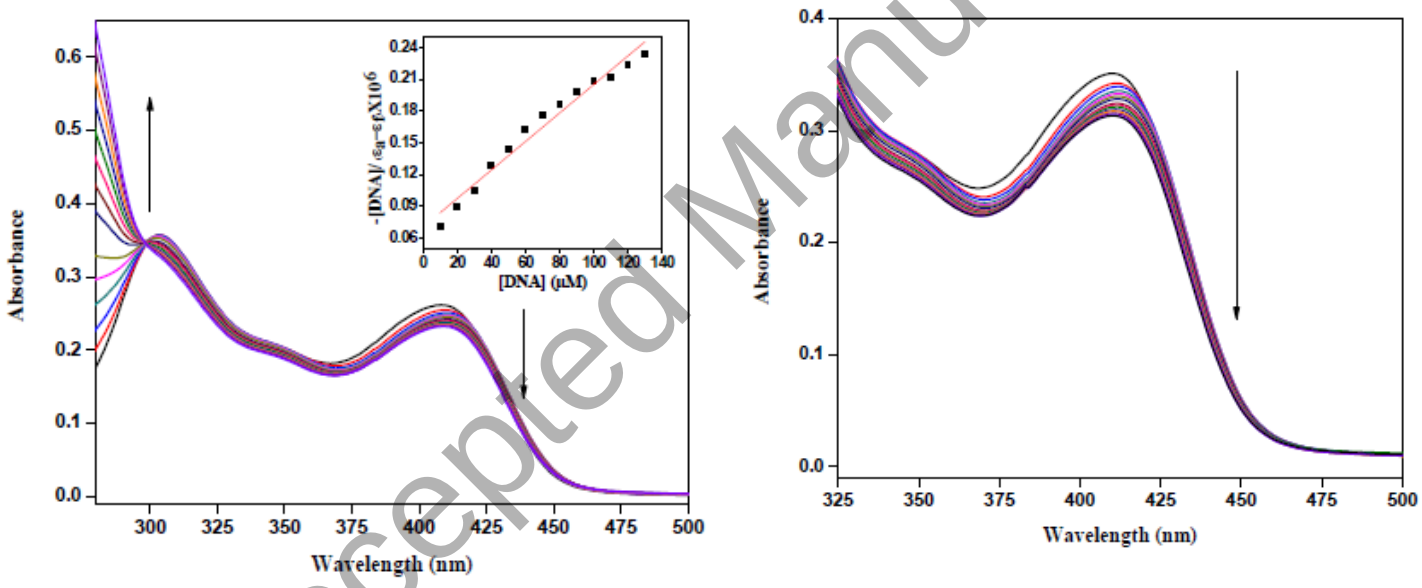

(B)

Figure 4. UV-Vis absorption spectra of complexes **1**(A) and **2**(B) in Tris-HCl buffer medium upon the titration of CT-DNA. [Complex] = 50 μM, [CT-DNA] = 10-140 μM. The arrow indicates the changes in absorbance with respect to an increase in the CT-DNA concentration. **Figure 4** (A) and (B) inset shows the linear fit of [DNA]/ [ε_a-ε_f] versus [DNA], for the calculation of intrinsic binding constant (K_b) of complexes **1** and **2** respectively. Decrease of absorption band intensity at 408 and 409 nm of complexes **1** and **2** respectively in Tris-HCl buffer upon addition of CT-DNA. [Complex] = 50 μM, [CT-DNA]

= 10-140 μM. The arrow indicates the changes in absorbance with respect to an increase in the CT-DNA concentration.

A prominent decrease in the absorption band intensity at 408 and 409 nm for the complexes **1** and **2** respectively were observed when incremental amount of CT-DNA were added to complexes **1** and **2**. Absorption spectra in Tris-HCl buffer medium with incremental addition of CT-DNA (0-110 μM) in absence of copper(II) complexes **1** and **2** were also carried out (Fig. S5). To determine the binding ability of complexes **1** and **2** with CT-DNA, the intrinsic binding constants (K_b) were calculated using the following equation (Fu et al., 2014; Wolfe, Shimer, Y& Meehan, 1987),

$$[DNA] / [\varepsilon_a-\varepsilon_f] = [DNA] / [\varepsilon_b-\varepsilon_f]+1/ K_b[\varepsilon_b-\varepsilon_f] \quad (1)$$

Where [DNA] is the CT-DNA concentration in base pairs, ε_a is the apparent extinction coefficient corresponds at a given concentration, and ε_b is extinction coefficient of the complex in fully bound form and ε_f is extinction coefficient of the complex in unbound form. Plotting [DNA] *versus* [DNA]/[ε_a-ε_f] gave a slope 1/[ε_a-ε_f] and a *y* intercept equal to 1/ K_b[ε_b-ε_f] respectively [Figure 4 inset]. Intrinsic binding constant, K_b values can be determined by monitoring the changes in the absorbance of the bands at 408 and 409 nm for **1** and **2** respectively with increasing concentration of DNA and is given by the ratio of the slope to the *y* intercept in the plots of [DNA] / [ε_a-ε_f] *versus* [DNA] (inset in Fig. 4). The intrinsic binding constants (K_b) were calculated as 1.36×10^4 and 1.15×10^4 M^{-1} for complexes **1** and **2** respectively. The calculated K_b values of complexes **1** and **2** also support the existence of moderate binding ability of the complexes to CT-DNA (Kathiresan, Mugesh, Murugan, & Annaraj, 2017; Biswas et al., 2017). The intrinsic binding constant (K_b) of complex **1** is greater than that of complex **2** with CT-DNA, which show that both complexes **1** and **2** moderately bind CT-DNA. The observed K_b values of complexes **1** and **2** are lower than that

of typical classical intercalator ethidium bromide (EB: $K_b = 1 \times 10^6$ M^{-1} (Pradeepa et al., 2015; Raman, & Jeyamurugan, 2009). The intrinsic binding constant (K_b) of previously reported related Schiff base metal complexes are in the range 10^3- 10^5 M^{-1} (Lian et al., 2016; Biswas et al., 2017; Chew, Lo, Sinniah, Sim, & Tan, 2014; Sathyadevi, Krishnamoorthy, Butorac, Cowley, & Dharmaraj, 2012; Reddy, Shilpa, Raju, & Raghavaiah, 2011). So, the complexes **1** and **2** bind to DNA with moderate binding ability (Fu et al., 2014).

Ethidium Bromide (EB) displacement study

DNA binding affinity of copper(II) complexes **1** and **2** were also studied by fluorescence spectroscopy using EtBr displacement titrations (Kathiresan, Mugesh, Murugan, & Annaraj, 2017; Gupta et al., 2013). Complexes **1** and **2** did not show any fluorescence at room temperature in the Tris-HCl buffer medium in presence of CT-DNA. When ethidium bromide binds with CT-DNA, then the EB-bound-DNA strongly fluoresce at about ~ 610 nm. Usually, high fluorescence is observed when EB is pre-treated with CT-DNA due to strong intercalative binding between adjacent DNA base pairs in the double helix. For this reason, EB is considered as the standard in intercalation study (Muralisankar, Sujith, Bhuvanesh, & Sreekanth, 2016; Jeyalakshmi et al., 2015). When another DNA binding compound is added then this very high fluorescence is quenched and the extent of quenching depends on the binding ability of the DNA-binding compound. For this reason competitive binding experiments were carried out to ascertain the binding mode of complexes by incremental variation of the concentration of the complexes **1** and **2** respectively (Haribabu et al., 2015; Guo, & Sadler, 1999; Dyson, & Sava, 2006; Orvig, & Abrams; Chitrapriya, Kamatchi, Zeller, Lee, & Natarajan, 2011; Lakowicz, & Webber, 1973; Baguley, & Lebret, 1984; Lepecq, & Paoletti, 1967). On addition of the copper(II) complexes **1** and **2** to EB bound CT-DNA

respectively, the emission intensity for both **1** and **2** at 607 nm were quenched by ~77.19% and ~71.93% respectively (Fig. 5).

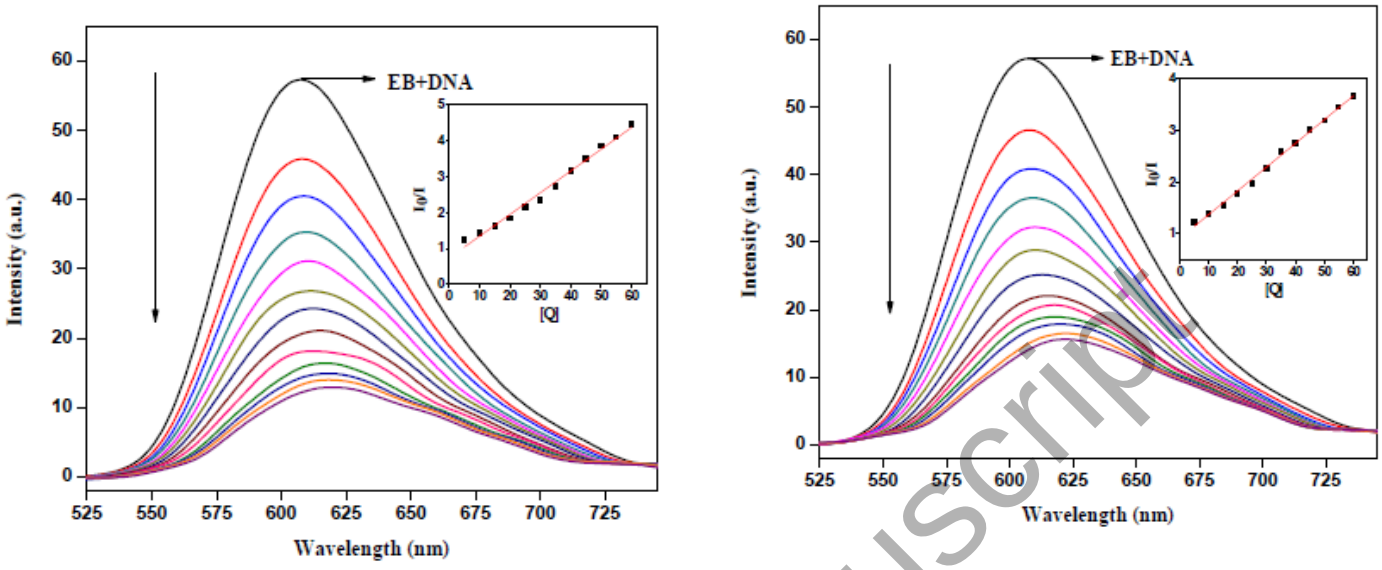

(A) (B)

Figure 5. Fluorescence emission spectra of ethidium bromide bound CT- DNA in the presence of complexes **1** (A) and **2** (B). [DNA] = 20 µM, [EB] = 10 µM and [Complex] = 0-65 µM. **Figure 5** inset shows plot the emission intensity I_0/I vs. [Q] for the determination of quenching constant of the complexes **1**and **2**.

The emission intensity of DNA pre-treated with EB decreased as the concentration of both **1** and **2** were increased gradually. It clearly indicate that both the complexes can replace EB from DNA-EB system (Fu et al., 2014; Chauhan, Banerjee, & Arjmand, 2007; Indumathy, Radhika, Kanthimathi, Weyhermuller, & Nair, 2007). According to previous literature, the significant quenching in the fluorescence spectra of ethidium bromide in presence of CT-DNA solution can be well explained by considering the intercalative binding mode of EB with DNA solution (Nanjundan et al., 2017, Zhao, Lin, Zhu, Sun, & Chen, 1998). The quenching extent of **1** and **2** were calculated using Stern-Volmer equation (Lian et al., 2016;

Biswas et al., 2017; Haribabu et al., 2015; Guo, & Sadler, 1999; Dyson, & Sava, 2006; Orvig, & Abrams; Lakowicz, 2013),

$I_0/I=1+K_{sv}[Q]$, (2)

where I_0 is the emission intensity in the absence of metal complex, I is the emission intensity in the presence of metal complex, K_{sv} is the linear Stern-Volmer quenching constant, and [Q] is the concentration of the metal complex. The ratio of the slope to the intercept obtained by plotting I_0/I *versus* [Q] yielded the value of quenching constant (K_{sv}) which corresponds to 6.044×10^4 M^{-1} and 4.592×10^4 M^{-1} for complexes **1** and **2** respectively (Fig. 5 inset). The mode of quenching process was evaluated by quenching rate constant (k_q) using the following equation (Mandegani, Asadi, Karbalaei-Heidari, Rastegari, & Asadi, 2016; Lakowicz, 2013),

$K_{sv} = \tau_0$ (3)

Where τ_0 is the life time of a fluorophore (~10^{-8} s). The quenching rate constant (k_q) of complex **1** is marginally higher than that of complex **2** and this fact also indicate relatively stronger quenching nature of complex **1**(Table 4).

Table 4. Stern-Volmer quenching constant (K_{sv}), quenching rate constant (k_q), binding constant (K_b), apparent binding constant (K_{app}) and number of binding sites (n) for the interactions of copper complexes **1** and **2** with CT-DNA solution.

Complexes	**K_{sv} (M^{-1})**	**k_q (M^{-1})**	**K_b (M^{-1})**	**K_{app} (M^{-1})**	**(n)**
(1)	6.044×10^4	6.044×10^{12}	1.360×10^4	4.445×10^5	1.11153
(2)	4.592×10^4	4.592×10^{12}	1.150×10^4	4.000×10^5	1.03487

The observed k_q value is in the order of 10^{12} which is greater than the limiting diffusion rate constant (2.0×10^{10} M^{-1} s^{-1}) for a biomacromolecule indicative of static quenching mechanism. In the static quenching mechanism, fluorophore and the quencher molecules form ground state complex (Mandegani, Asadi, Karbalaei-Heidari, Rastegari, & Asadi,

2016). Further, the apparent binding constant (K_{app}) values were calculated for **1** and **2** using the following equation (Alagesan, Sathyadevi, Krishnamoorthy, Bhuvanesh, & Dharmaraj, 2014),

$$K_{EB}\,[EB] = K_{app}\,[complex] \qquad (4)$$

Where K_{EB} is $1.0 \times 10^{6}\ M^{-1}$ (Chew, Lo, Sinniah, Sim, & Tan, 2014; Pradeepa et al., 2015) and EB concentration is 10 µM; [complex] is the concentration of the complex causing 50% decrease in emission intensity of EB. The apparent binding constants (K_{app}) of the copper (II) complexes **1** and **2** are shown in Table 4. The observed K_{app} values for complexes **1** and **2** are smaller than that of classical intercalator ethidium bromide (EB). From the above mentioned data, it is clear that complex **1** can more effectively replace EtBr than complex **2** which is in agreement with the results obtained from the UV-Vis spectral studies. The number of binding sites (n) of complexes **1** and **2** were also obtained by using Scatchard equation (Kalaivani et al., 2014),

$$\log [(I_0\text{-}I)/I] = \log K_b + n \log [Q] \qquad (4)$$

From the slope of plot of log $[(I_0\text{-}I)/I]$ *versus* log [Q] (Fig. S6), the number of binding sites (n) of two copper (II) complexes **1** and **2** were determined (Table 4).

Electrochemical study

Cyclic voltammetry is now a days considered as very useful analytical method to determine the redox behaviour of metal complexes in presence of biologically active molecules (Mandegani, Asadi, Karbalaei-Heidari, Rastegari, & Asadi, 2016; Srinivasan, Annaraj, & Athappan, 2005; Banerjee et al., 2009). It is also one of the important tools to determine the mode of interaction between metal complexes and DNA molecule. The variation in peak current with variation of DNA concentration at fixed concentration of metal complexes **1** and **2** were used to determine the binding parameters. Cyclic voltammograms of complexes **1** and **2** are shown in Figure 6.

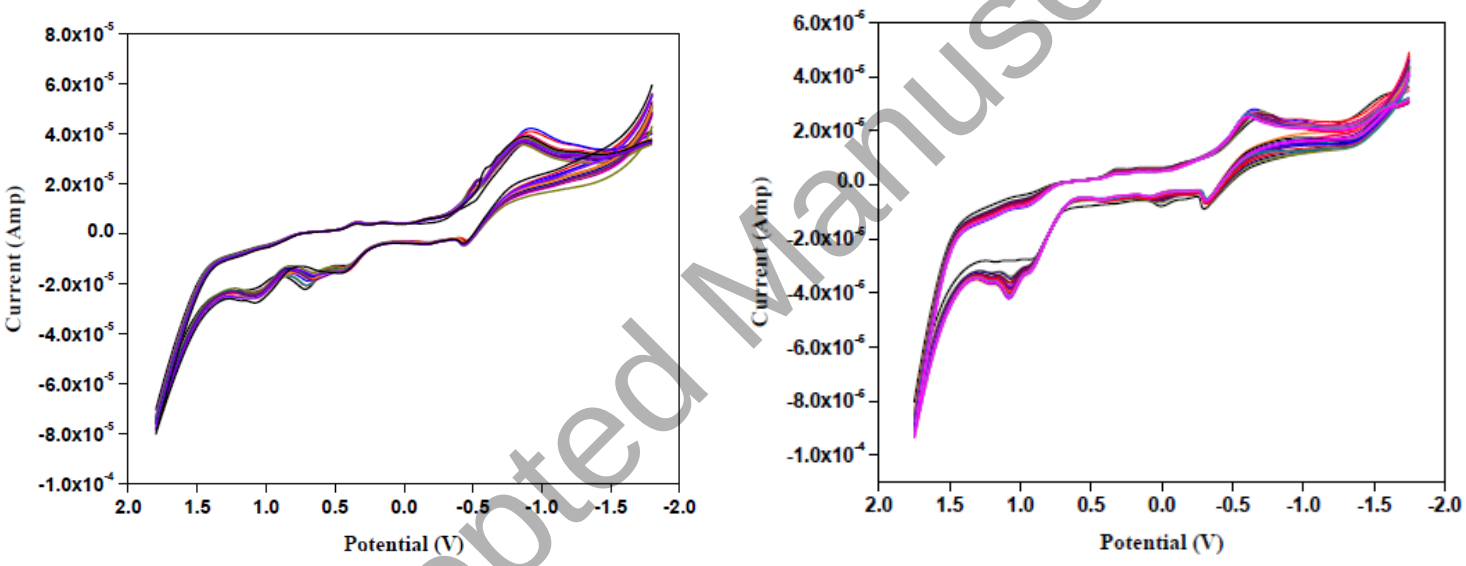

(A) (B)

Figure 6. The cyclic voltammograms of complexes **1**(A) and **2** (B) (1 mM) in the absence and in presence of various concentration of CT-DNA solution.

Both complexes **1** and **2** in Tris-HCl buffer medium exhibit one oxidative potential wave in anodic region and one reductive potential wave in cathodic region. Complex **1** also showed a Schiff bade oxidation peak in anodic region. After addition of CT-DNA to the solution of copper(II) complexes **1** and **2**, the oxidative waves at 0.47 (versus SCE) for **1** and 0.92 V

(versus SCE) for **2** were shifted to more positive potential value at 0.71 and 1.07 V respectively. Similarly, the reductive waves at -0.88 and -0.69 V for complexes **1** and **2** respectively were also shifted towards comparatively less negative potential value of -0.87 and -0.60 V. The above observation signifies that electron deficiency exists due to some sort of interaction between copper (II) complexes and the base pairs of DNA (Biswas et al., 2017; Banerjee et al., 2009). This shift in the anodic and cathodic peak potentials towards more positive side clearly show that the reduced forms of both **1** and **2** interact more strongly than their oxidised forms.

Viscosity study

Photo-physical titrations generally provide necessary information, but not provide satisfactory evidence to support the binding mode of the complexes with DNA. Viscosity measurement is often considered as an effective way to determine the binding mode between small molecules and DNA. For intercalation binding between metal complexes and the base pairs of DNA forces these base pairs away to stay from each other and therefore, unwinding the double helix and lengthening a given amount of DNA which in turn, increases the viscosity of the DNA solution. In contrast, a partial and/or non-intercalation of the metal complexes can result a less pronounced effect on the viscosity (Lu et al., 2014; Gabbay, Scofield, & Baxter, 1973). Here, viscosity measurements were performed by determining viscosity of CT-DNA (100 µM) in Tris-HCl-buffer medium at pH 7.2 with incremental increase of complex **1** or complex **2** (10-60 µM). The relative viscosities of CT-DNA in the presence of the complexes **1** and **2** respectively are shown in Figure 7.

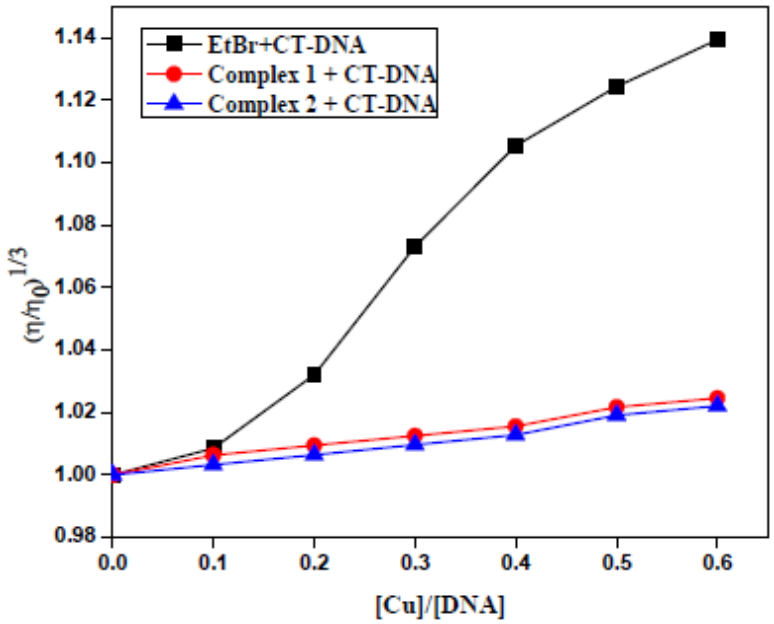

Figure 7. Relative specific viscosity increment of CT-DNA with complexes **1** and **2**. Complexes **1** and **2 (**10-60 µM) in the presence of fixed concentration of CT-DNA solution (100 µM) at 27°C.

Relative specific viscosity $(\eta/\eta_0)^{1/3}$ were plotted against 1/R (where R= [DNA base pairs]/[Cu]) (Jaividhya, Ganeshpandian, Dhivya, Akbarsha, & Palaniandavar, 2015). The CT-DNA viscosity exhibits a small increase in the presence of increasing amounts of both the metal complexes **1** and **2**. The relative viscosities of CT-DNA solutions containing complexes **1** and **2** respectively increase slightly with the slope values varies from 0.29 to 0.28, while the viscosity of the CT-DNA solution in presence of ethidium bromide increase steadily with a slope of 0.97. The slope values obtained from viscommetric titrations was obtained as 0.28-0.29 which are very similar with the previously reported related Cu(II) thiosemicarbazone complex (Biswas et al., 2017). The relative viscosity of a typical classical intercalator EtBr is much higher than the viscosity of CT-DNA in presence of complexes **1** and **2** (Biswas et al., 2017; Yilmaz et al., 2017; Li, Zhao, & Wu, 2006). The binding constants of **1** and **2** obtained from spectrophotommetric analysis (UV-Vis and fluorescence spectral studies) are much lower than that of EB. These results suggest that increase of viscosity of CT-DNA for complexes **1** and **2** are less in comparison with ethidium bromide

because of smaller binding constants of copper (II) complexes (Biswas et al., 2017; Yilmaz et al., 2017).

Protein binding studies

Electronic absorption titration

Metal complex binding with serum albumins is of great importance now a days as these complex-albumin binding influence absorption, drug transport and other properties in vivo (Kalaivani et al., 2014; Zhang et al., 2010). To investigate the protein-metal complex relationship, bovine serum albumin (BSA) as well as human serum albumin (HSA) are widely used for this purpose due to their similar structural parameters (Ingle et al., 2015; Ganeshpandian et al., 2013; Raja et al., 2011). UV-Vis absorption method is an unique method to explore the changes in structure and also the type of quenching that occurs (dynamic or static quenching). For a dynamic quenching mechanism, the absorption spectral position of the substance remains unchanged and only the excited state fluorescence molecule is influenced by quenchers, whereas, for static quenching, generally one new compound is formed between the ground state of the molecule and quencher which results considerable change in absorption spectra (Poornima, Gunasekaran, & Kandaswamy, 2015; Eftink, & Ghiron, 1976). The absorption spectra of BSA and HSA in presence of the **1** and **2** were presented in Figures 8 and S7 respectively.

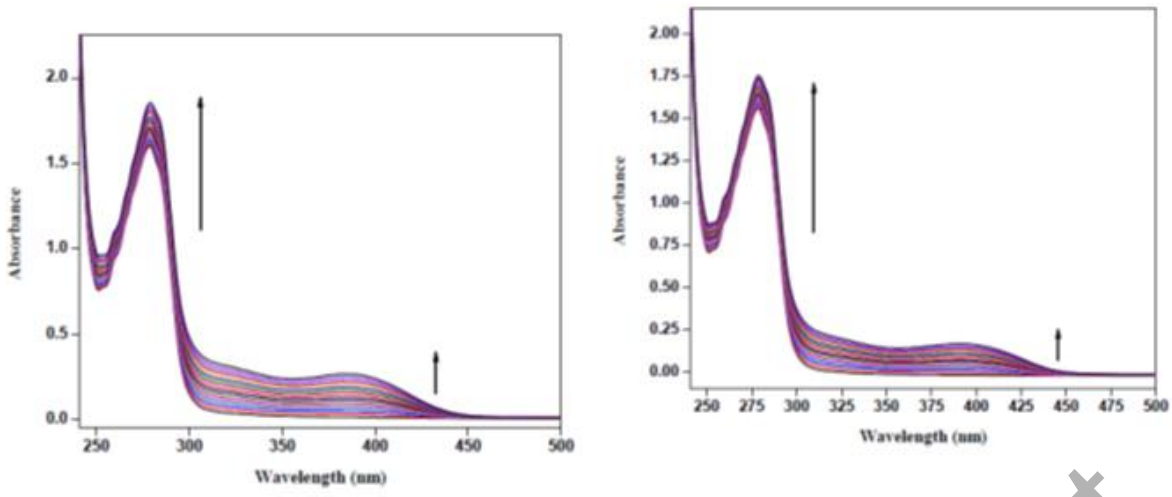

(A) (B)

Figure 8. UV-Vis absorption spectra of BSA [40 µM] in Tris-HCl buffer medium and BSA with increasing concentration [0-70] of complexes **1**(A) and **2**(B) at room temperature.

The absorption bands for BSA and also for HSA were observed at 279 nm in the absence of **1** and **2**. Both of them showed an increase in absorption intensity after incremental addition of complexes **1** and **2** respectively. Absorption intensity of both BSA and HSA increases without any change in absorption band position. This fact clearly indicate that the interaction between complexes **1** and **2** with serum albumins (BSA and HSA) involved static quenching process (Muralisankar, Sujith, Bhuvanesh, & Sreekanth, 2016; Sathyadevi, Krishnamoorthy, Butorac, Cowley, & Dharmaraj, 2012; Raja et al., 2011; Sathyadevi et al., 2011).

Fluorescence quenching study

Interactions of metal complexes with serum albumins are important to study. Both BSA and HSA are used in fluorescence quenching study due to their similar structural environment. Fluorescence quenching refers to any process in which fluorescence intensity of a substance

decreases due to a variety of molecular interactions present. Interaction of serum albumins (both BSA and HSA) with complexes **1** and **2** were studied at room temperature. For this

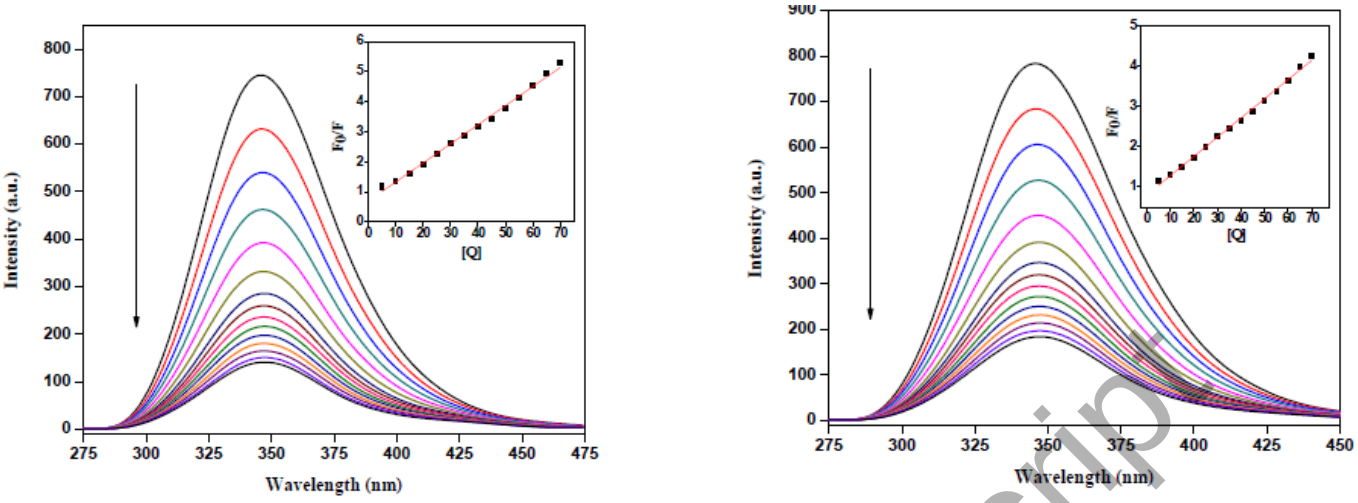

study, BSA and HSA (40 μM) were taken and both were titrated with incremental increase of complexes **1** and **2** concentrations (0-70 μM) (Fig. 9 and S8).

(A) (B)

Figure 9. The emission spectra of BSA (40 μM: λexi = 279 nm: λemi = 345 nm) as a function of concentration of complexes **1**(A) and **2**(B) (0-70 μM)**.** The arrow indicates the effect of metal complexes on the fluorescence emission of BSA. The inset shows Stern-Volmer linear plot of F^0/F vs. [Q] of the complexes **1** and **2** with BSA.

When fluorescence titrations were carried out by incremental addition of complexes **1** and **2** to proteins, a significant decrease in the fluorescence intensity was observed at 345 nm for BSA and 343 nm for HSA along with hypochromism. The observed quenching in fluorescence intensity shows binding of complexes **1** and **2** to protein molecules (Kalaivani et al., 2014; Wang, Zhang, Zhang, Tao, & Tang, 2017). The fluorescence quenching mechanism for the complex-protein system can be observed from the fluorescence quenching data using the classical Stern-Volmer equation (Fu et al., 2014; Lakowicz, 2013),

$F^0/F = 1+K_{sv}[Q] = 1+ k_q \tau_0$ (5)

where F_0 and F represent the fluorescence intensities in the absence and presence of a quencher, respectively. K_{sv}, k_q, τ_0 and [Q] are linear Stern-Volmer quenching constant, the quenching rate constant of biomolecules, the average lifetime of biomolecules without a quencher ($k_q = 10^{-8}$ s) and the concentration of the quencher, respectively. The K_{sv} values **1** and **2** were determined from the slope of the plot of F_0/F *versus* [Q] (Fig. 9 and S8 inset for BSA and HSA respectively) and k_q values were obtained from the equation $K_{sv}= k_q \tau_0$ and are shown in Table 5.

Table 5. Stren-Volmer quenching constant (K_{sv}), quenching rate constant (k_q), binding constant (K_b) and number of binding sites (n) for the interactions of copper complexes **1** and **2** with both BSA and HSA.

Complexes	Protein molecules	K_{sv} (M^{-1})	k_q (M^{-1})	K_b (M^{-1})	(n)
(1)	BSA	6.309×10^4	6.309×10^{12}	4.992×10^5	1.21997
(1)	HSA	7.567×10^4	7.567×10^{12}	14.209×10^5	1.31275
(2)	BSA	4.285×10^4	4.285×10^{12}	4.006×10^5	1.23578
(2)	HSA	4.771×10^4	4.771×10^{12}	5.131×10^5	1.24851

The quenching rate constant (k_q) value is about 100 times higher than optical collision rate constant, 2×10^{10} M^{-1} for both **1** and **2**. (Rambabu, Kumar, Tejaswi, Vamsikrishna, & Shivaraj, 2016; Pradeepa et al., 2015; Eftink, 1991). These results indicate that both **1** and **2** interact strongly with protein molecules by static quenching process. (Rambabu, Kumar, Tejaswi, Vamsikrishna, & Shivaraj, 2016; Fu et al., 2014; Das, Nasani, Saha, Mobin, & Mukhopadhyay, 2015; Samari, Hemmateenejad, Shamsipur, Rashidi, & Samouei, 2012). Table 5 shows the higher Stern-Volmer quenching constants and quenching rate constants for

the complexes **1** and **2** with BSA and HSA. The binding constant (K_b) and the number of binding sites (n) can be obtained according to the fluorescence titration method using the Scatchard equation (Rambabu, Kumar, Tejaswi, Vamsikrishna, & Shivaraj, 2016; Fu et al., 2014; Samari, Hemmateenejad, Shamsipur, Rashidi, & Samouei, 2012),

$$\log [(F_0\text{-}F)/F] = \log K_b + n \log[Q] \qquad (6)$$

Where, in the present case, K_b is the binding constant for protein-complex interaction and (n) is the number of binding sites per BSA and HSA molecules, which can be determined by the slope and the intercept of the double logarithm regression curve of log $[(F_0\text{-}F)/F]$ *versus* log[Q] (Fig. S9 and S10; Table 5).

Cytotoxic profile study

Cytotoxicity of complexes 1 and 2 in normal cells

Data (Fig. S11) from hemolytic assay reveals that complex **1** do not show significant haemolysis upto a concentration of 10µg/mL. Percentage of haemolysis increases quite significantly beyond 10µg/mL. However, complex **1** exhibited haemolysis greater than 10% beyond 5µg/mL. Both **1** and **2** proved to be cytotoxic beyond a dose of 0.3µg/mL in nucleated cells as determined by Trypan blue exclusion method in human PBMC by complex **1** and **2** which are shown in Figure 10.

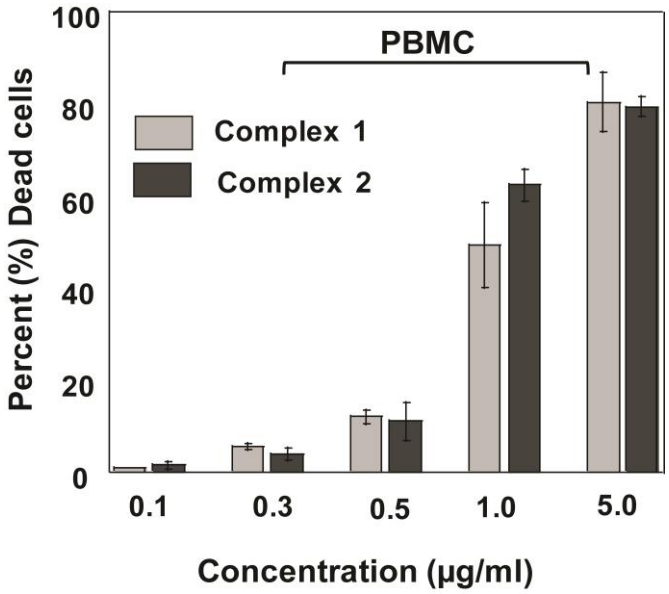

Figure 10. Effect of treatment of **1** and **2** on percentage PBMC viability measured by Trypan Blue exclusion method.

Determination of IC_{50} in cancer cell lines by MTT Assay

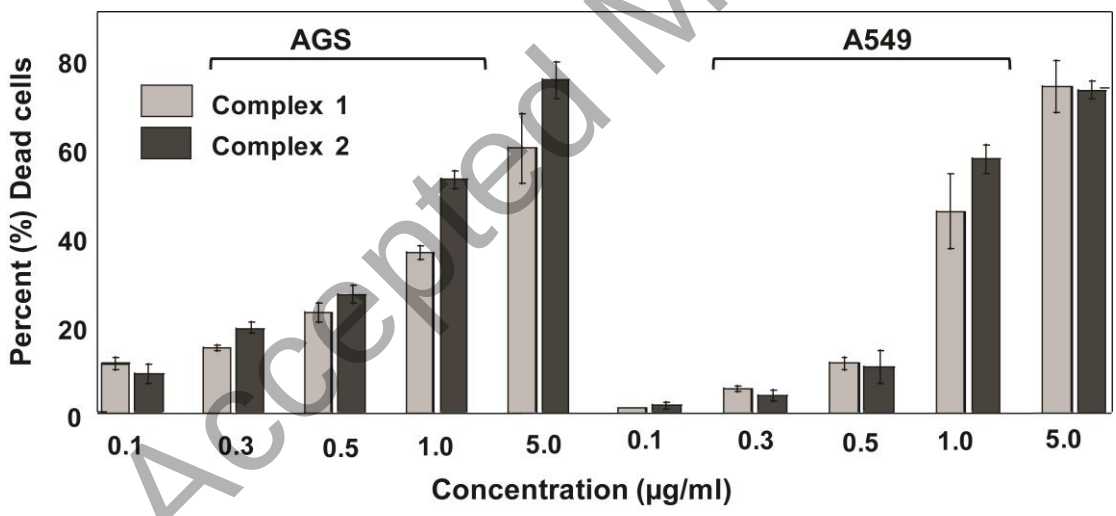

Figure 11. Effect of treatment of **1** and **2** on A549 and AGS cell viability measured by MTT assay at various concentration of **1** and **2**.

MTT (Figure 11) assay revealed that the cytotoxicity of complex **1** in A549 and AGS cells in a concentration dependent manner. More than 50% killing was observed at a concentration of

5.0µg/mL for AGS and 1.0 µg/mL for A549. Complex **2** shows similar high concentrations for 50 % for both the cell lines i.e approximately 1.0 µg/mL. The IC_{50} values are 11.098 µM for AGS and 2.20 µM for A549 for **1** and 2.34 µM for AGS and 2.34 µM for A549 for **2** respectively.

IC_{50} of both complexes **1** and **2** for AGS and A549 were well above the tolerance dose found in case of hemolytic data or from that of human PBMC. As mentioned above, 0.5 µg/mL is comparatively less toxic to normal cells and is able to induce more than 50% killing in cancer cells especially for AGS cells. For this reason we have selected 0.5 µg/ml concentration for further studies on cancer cells for both complexes **1** and **2**.

Analysis of Cell Cycle Phase Distribution of cancer cells

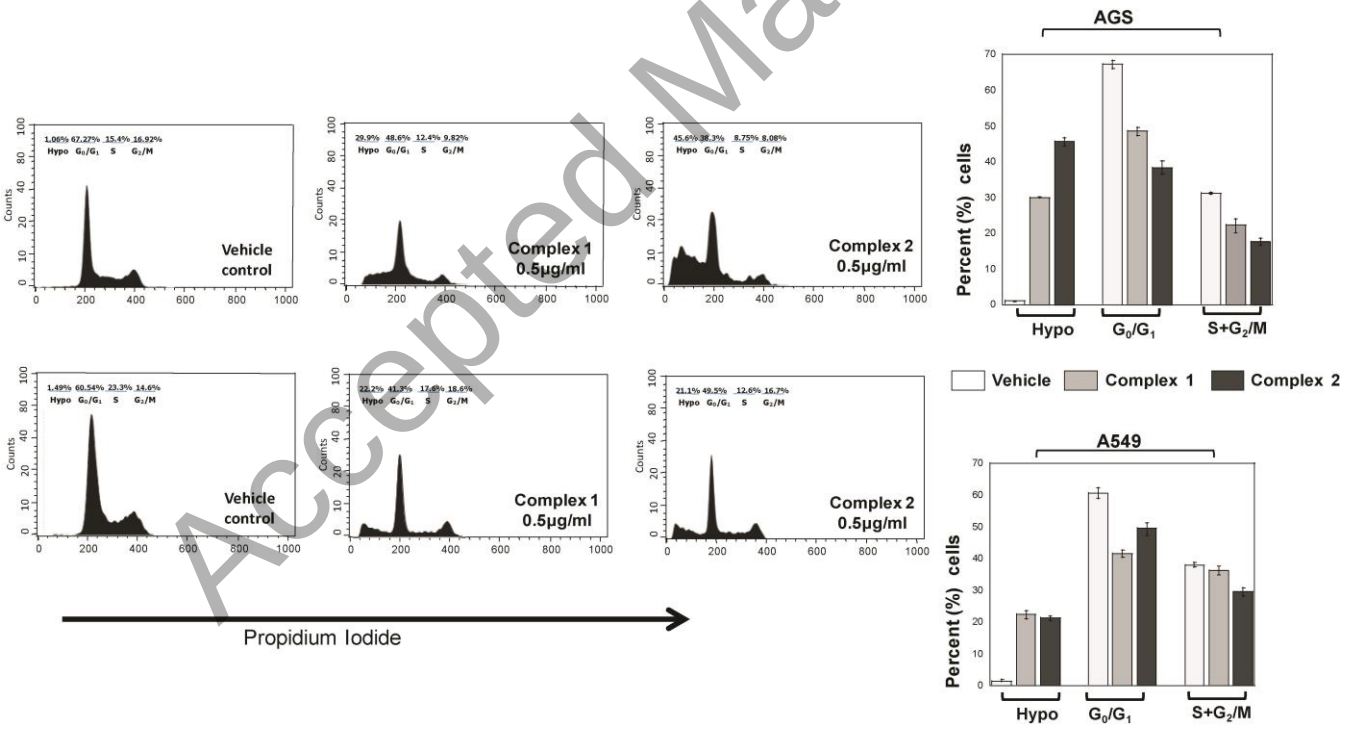

Figure 12. Effect of treatment of **1** and **2** on AGS and A549 cell cycle. Cell cycle analysis of treated and untreated AGS and A549 cells by Flowcytometer using propidium iodide (PI) as DNA-binding fluorochrome. A. Histogram display of DNA content (x-axis, PI-fluorescence)

versus counts (y-axis) has been shown. B. Bar diagram representation of cell cycle phase distribution of AGS from different experimental groups.

As shown in Figure 12 treatment with complexes **1** and **2** resulted in a significant increase in the sub-G0 region in both AGS and A549 cells (hyperploidy population). Interestingly cell cycle data also revealed that AGS was more susceptible to both the complexes **1** and **2** as compared to A549. In case of complex **1**, sub-G0 phase is 29.9 ± 0.83% for AGS and 20.05 ± 1.20% for A549. Similarly in case of complex **2**, sub-G0 phase is 45.6 ± 1.17% for AGS and 20.5 ± 0.42% for A549. This means complex **2** shows better efficiency in cancer cell reduction as compared to complex **1**. However both the complexes **1** and **2** are of equal potency in reduction of A549 though lesser as compared with AGS.

Effect of complexes 1 and 2 in AGS and A549 apoptosis

In order to confirm the increase in apoptotic induction by complexes **1** and **2**, we performed annexin V/PI assay in all the groups by staining the AGS and A549 cells with FITC tagged annexin V and PI and measuring the fluorescence intensity in a flowcytometer.

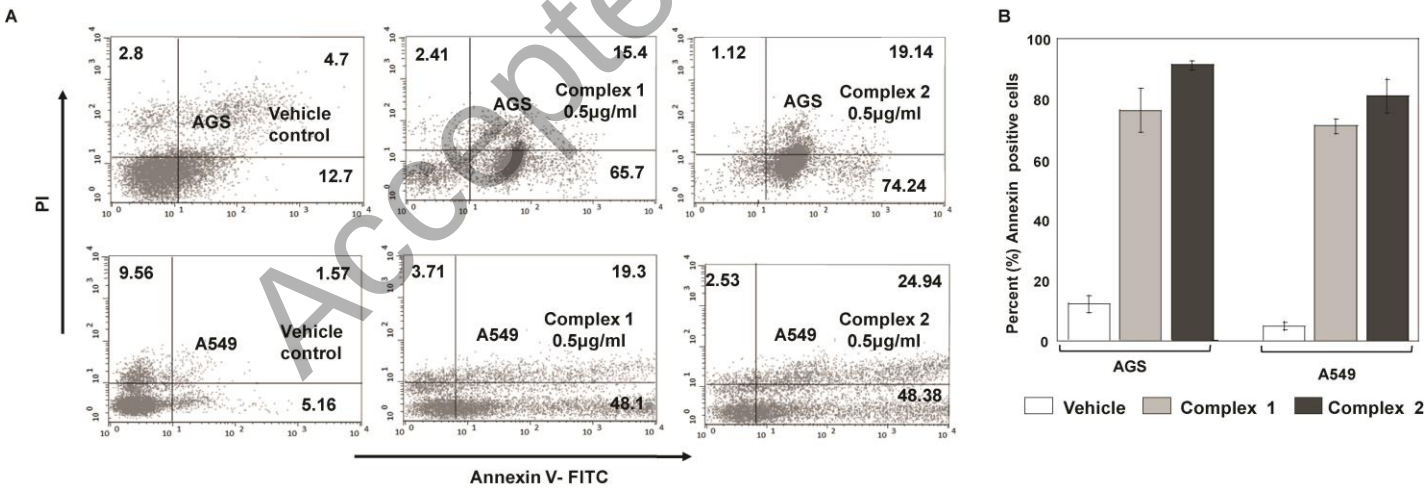

Figure 13. Effect of treatment of **1** and **2** on AGS and A549 cells with regard to Annexin V/PI binding. (A) Annexin V Assay in AGS and A549 cells. Dual parameter dot plot of FITC-fluorescence (x-axis) versus PI-fluorescence (y-axis) has been shown in logarithmic fluorescence intensity. Quadrants: lower left, live cells; lower right, apoptotic cells; upper

right, necrotic cells. (B) Bar diagram representation of percent Annexin V positive AGS cells and A549 cells from different experimental groups are also given.

Results suggest a significant increase in the percentage of annexin positive cells upon treatment of either of the complexes **1** and **2** as compared to control counterparts. A prominent increase is about 81.3 ± 5.09% and 67.4 ± 1.13% for complex **1** and 93.38 ± 0.98% and 73.32 ± 0.09% for complex **2** in AGS and A549 respectively. The data confirmed the killing pattern as found in cell cycle analysis. AGS was more susceptible to either of the complexes **1** and **2** as compared to that of A549 (Fig. 13).

Western Blot analysis of protein expressions

Further analysis on important protein marker like anti-apoptotic protein Bcl-2, pro-apoptotic protein Bax and p53, cell proliferation associated marker PCNA (proliferating cell nuclear antigen) and executioner caspase 3.

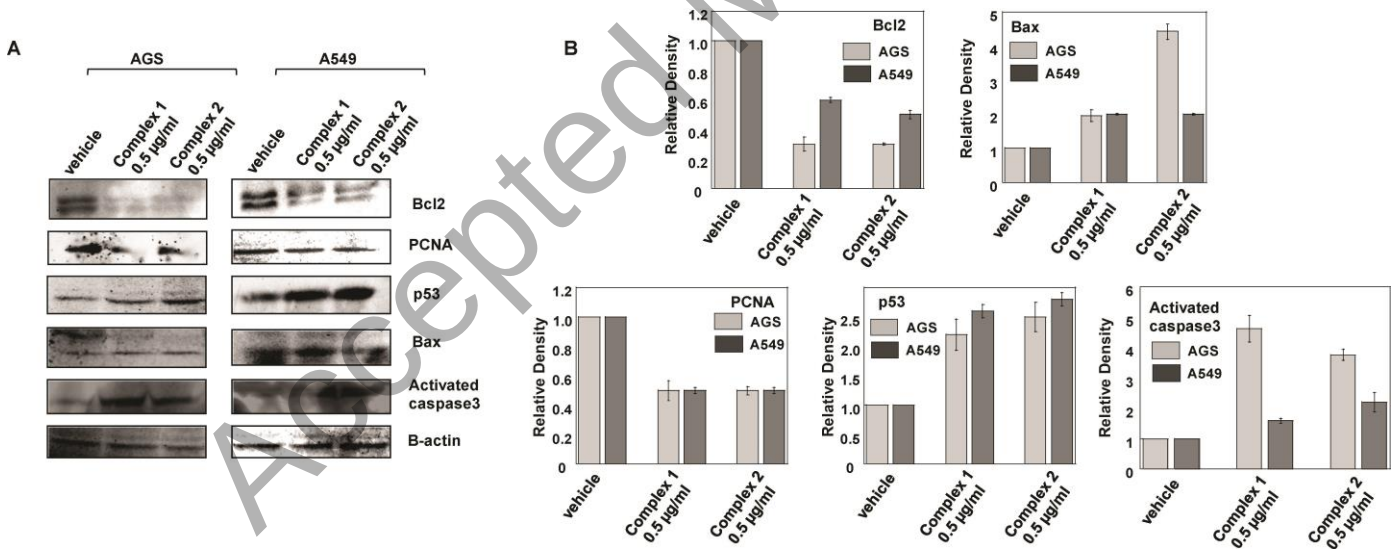

Figure 14. Effect of treatment of **1** and **2** on AGS and A549 protein expressions. (A) Western Blot detection of Bcl-2, pro-apoptotic protein Bax and p53, cell proliferation associated marker PCNA (proliferating cell nuclear antigen) and executioner caspase 3. Equal loading of

protein in the lanes was confirmed by B-actin. (B) Indicated proteins are represented as bar diagrams of mean + SD of their relative densities as measured from three independent experiments.

Western blot of the above proteins revealed both complexes **1** and **2** successfully decreased anti-apoptotic protein Bcl-2, increased pro-apoptotic protein Bax and p53, decreased cell proliferation associated marker PCNA (proliferating cell nuclear antigen) and increased the expression of executioner caspase 3 in both AGS and A549 cells (Fig. 14).

Molecular docking studies

Docking involves the calculation of the ligand orientation in the active site and/or binding site, and can be used to predict the residues that could be involved in substrate/inhibitor binding. It is an algorithm that determines the binding site of a protein molecule. This includes determining the orientation of the compound, its conformational geometry, and the scoring. In order to gain better insight into the nature of macromolecule-ligand binding, molecular docking study of copper complexes with HSA (PDB ID: 4IW2), BSA (PDB ID: 4F5S) and the DNA duplex of sequence d(CGATCG)2 (PDB ID: 1Z3F) were performed.

Molecular docking studies of complexes 1 and 2 with duplex DNA

In this study, the synthesized complexes were docked to the duplex DNA to investigate the binding mode. The conformations of the docked complexes were analyzed in terms of interaction energy, hydrophobic interaction, and hydrogen bonding between synthesized complexes and duplex DNA (PDB ID: 1Z3F). The complex **1** forms one hydrogen bond and seven hydrophobic interactions with the CDOCKER interaction energy of -47.0462 kcal/mol (Fig. 15 and Table 6) whereas complex **2** gains its stability by forming five hydrogen bond

and two hydrophobic interactions with CDOCKER interaction energy of - 45.8947kcal/mol (Fig. S12 and Table 7).

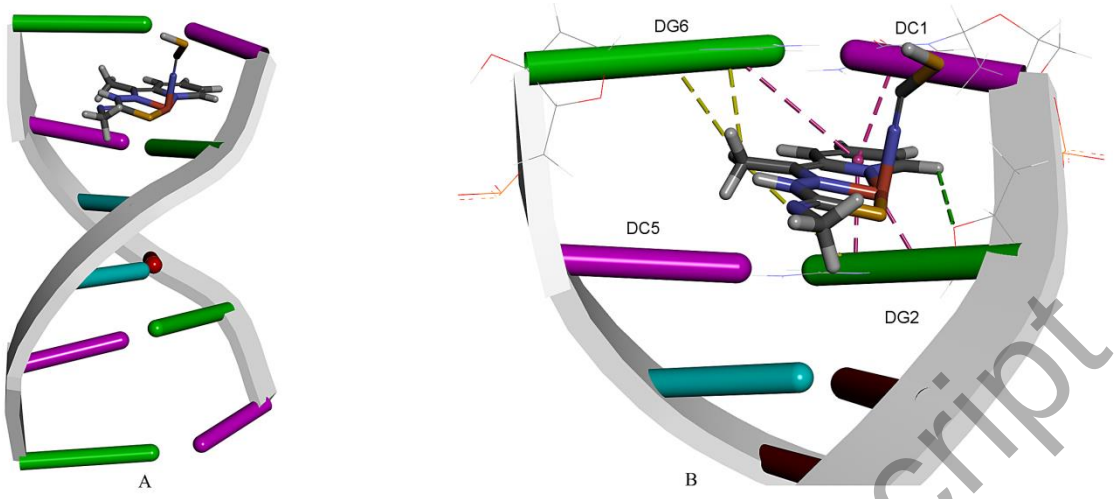

Figure 15. A molecular docked model of complex **1** with the duplex DNA hexamer (PDB ID: 1Z3F). (A) The full view of docking between complex **1** and 1Z3F. (B) The binding mode between complex **1** and 1Z3F. Green, pink, and yellow dashed line represents hydrogen bond, pi-pi stacked and pi-alkyl interactions respectively.

It was clearly observed from the docking study that both the synthesized compounds binds with the DNA molecule moderately as supported from the experimental study.

Table 6. Molecular interaction of complex **1** with DNA.

Sl no.	Bond Type	Interaction Constituent	Distance (Å)
1	H-bond	Complex1:H10 - A:DG2:O4'	3.07
2	Pi-Pi stacked	Complex1 - A:DC1	4.03
3	Pi-Pi stacked	Complex1 - A:DG2	3.90
4	Pi-Pi stacked	Complex1 - A:DG2	3.41
5	Pi-Pi stacked	Complex1 - B:DG6	5.29
6	Pi-alkyl	Complex1:C19 - A:DG2	4.96
7	Pi-alkyl	Complex1:C19 - B:DG6	5.06
8	Pi-alkyl	Complex1:C19 - B:DG6	4.06

Table 7. Molecular interaction of complex **2** with DNA.

Sl no.	Bond Type	Interaction Constituent	Distance (Å)
1	H-bond	Complex2:N22 - A:DG2:H21	2.80
2	H-bond	Complex2:N22 - A:DG2:H22	2.63
3	H-bond	Complex2:H63 - B:DC5:O2	2.16
4	H-bond	Complex2:H50 - B:DG6:O4'	2.77
5	H-bond	Complex2:H68 - B:DG6: O4'	2.50
6	Pi-alkyl	Complex2:C17 - A:DG2	4.66
7	Pi-alkyl	Complex2:C17 - A:DG2	4.00

Molecular docking studies of complexes 1 and 2 with BSA

The binding mode of complex **1** at the IB subdomain of BSA showed various interactions which include van der Waals, electrostatic and pi-cation with the key residues in close +, Leu189, Ala193, Arg196 residues for van der Waals and Asp108, Ser109, Arg144, His145, Ser192, Glu424, Arg458 residues for electrostatic interactions. It forms two pi-cation interactions with the amino acids His145 and Arg458 of the BSA protein (Fig. 16B).

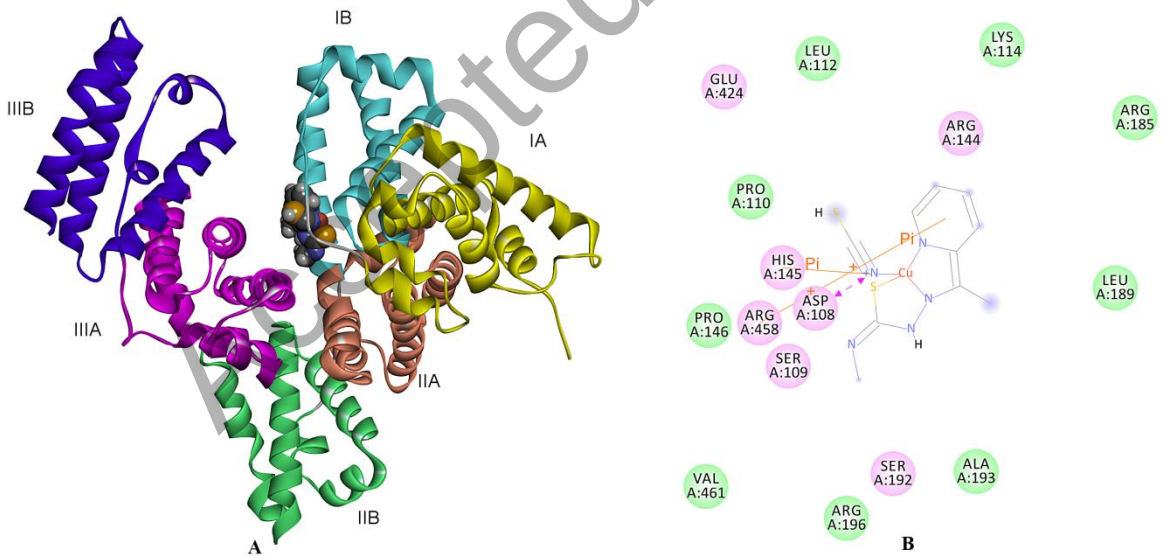

Figure 16. Docking of complex **1** in the binding site of BSA (PDB ID: 4F5S). (A) The full view of BSA-complex **1** system. Representation of complex **1** in CPK mode. (B) 2D representation of intermolecular interaction of BSA with complex **1**. Residues involved in electrostatic and van der Waals interactions are represented by pink and green circles respectively. Orange line shows pi-cation interaction between BSA and complex **1**.

The second ligand, complex **2** was encompassed into the cavity of IIIA-IB subdomain of the BSA protein with the binding energy of 0.7821 kcal/mol (Fig. S13A and Table 10) and formed one hydrogen bond with Arg458. The residues involved in van der Waals interactions were Pro110, Asp111, Leu112, Pro113, Lys114, Leu115, Glu140, Ile141, Pro146, Val188, Leu189, Ser192, Ala193, Arg196, Leu462 and Asp108, Ser109, Arg144, His145, Arg185, Glu424, Arg458 were involved in electrostatic interactions (Fig. S13B and Table 8).

Table 8. Molecular interaction of synthesized complexes **1** and **2** with BSA.

Ligands	H-bond	Van der waals	Electrostatic	Pi-cation
Complex **1**	-	Pro111, Leu112, Lys114, Pro146, Arg185, Leu189, Ala193, Arg196	Asp108, Ser109, Arg144, His145, Ser192, Glu424, Arg458	His145, Arg458
Complex **2**	Arg458	Pro110, Asp111, Leu112, Pro113, Lys114, Leu115, Glu140, Ile141, Pro146, Val188, Leu189, Ser192, Ala193, Arg196, Leu462	Asp108, Ser109, Arg144, His145, Arg185, Glu424, Arg458	Lys114, Arg144, Arg185, Arg458

It was observed from the binding energy study that the complex **1** has the higher binding affinity than the complex **2** molecule.

Molecular docking of complexes 1 and 2 with HSA

Crystal structures of both HSA and BSA indicate that both protein molecules consist of three major domains (I-III): I (1-195), II (196-383) and III (384-585); each domain composed of two subdomains (A and B) that resemble a heart-shaped molecule. The lowest binding energy (-91.7575 kcal/mol) pose (Fig. 17A and Table 10) of complex **1** with HSA was present within the cavity of subdomains IIA and IIB. The residues of HSA that are involved in van der Waals interactions are Ala210, Ala213, Lys323, Leu347, Ala350, Lys351, Arg358, Val482; while those that are involved in electrostatic interactions are Arg209, Asp324, Leu327, Gly328, Leu331, Glu354. It was observed that the complex **1** exhibited one pi-cation interaction with Lys351 of HSA protein (Fig. 17B).

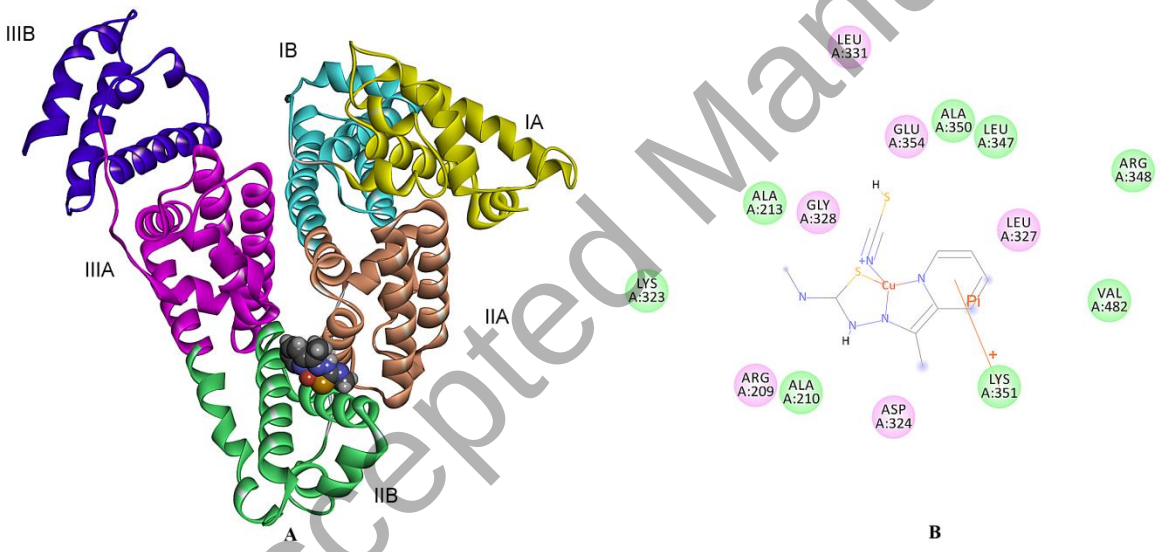

Figure 17. Docking of complex **1** in the binding site of HSA (PDB ID: 4IW2). (A) The full view of HSA-complex **1** system. Representation of complex **1** in CPK mode. (B) 2D representation of intermolecular interaction of HSA with complex **1**. Residues involved in electrostatic and van der Waals interactions are represented by pink and green circles respectively. Orange line shows pi-cation interaction between HSA and complex **1**.

The complex **2** fits into the cavity of IIA-IB subdomain of HSA with the binding energy of -2.0727 kcal/mol (Fig. S14A and Table 10) and formed one hydrogen bond with Lys195. The

non-covalent van der Waals contribution present within the binding pocket of HSA are contributed by Tyr150, Glu153, Glu188, Ala191, Ser192, Lys199, His288 whereas residues Lys195, Arg218, Arg222, Arg257, Ala291, Glu292, Glu294, and Lys444 are responsible for electrostatic interactions. Furthermore, the formation of two extensive pi-cation interactions with the amino acids Lys195 and Arg257, which played an important role in stabilizing the complex **2**-HSA system (Fig. S14B and Table 9). It was clear from the binding energy that the complex **1** strongly binds with the HSA than complex **2**.

Table 9. Molecular interaction of synthesized complexes **1** and **2** with HSA.

Ligands	H-bond	Van der waals	Electrostatic	Pi-cation
Complex **1**	-	Ala210, Ala213, Lys323, Leu347, Ala350, Lys351, Arg358, Val482	Arg209, Asp324, Leu327, Gly328, Leu331, Glu354	Lys351
Complex **2**	Lys195	Tyr150, Glu153, Glu188, Ala191, Ser192, Lys199, His288	Lys195, Arg218, Arg222, Arg257, Ala291, Glu292, Glu294, Lys444	Lys195, Arg257

Table 10. Energy values of docked complexes **1** and **2**.

Ligands	HSA		BSA	
	CDOCKER interaction energy (kcal/mol)	Binding energy (kcal/mol)	CDOCKER interaction energy (kcal/mol)	Binding energy (kcal/mol)
Complex **1**	-28.3393	-91.7575	-26.0297	-8.6158
Complex **2**	-3.3311	-2.0721	-1.0724	0.7821

Conclusion

The following are the salient observations and findings of the present work:

a) The current research work focuses on the synthesis and characterization of two new copper (II) substituted thiosemicarbazone complexes along with thiocyanate as bridging ligand. Complexes **1** and **2** were characterized by structural, analytical as well as spectral methods.

b) In order to determine the potential binding ability of **1** and **2**, CT-DNA and protein molecules (BSA and HSA) were taken as model. Both the complexes showed effective DNA propensity. The DNA binding ability of **1** and **2** were determined using UV-Vis, fluorescence spectral titration, viscosity study and cyclic voltammetric measurements. Complexes **1** and **2** bind to DNA moderately and corresponding quenching is found as static quenching.

c) Complexes **1** and **2** bind to serum albumins (BSA and HSA) and both are responsible for quenching of protein molecules by a static quenching pattern. The static quenching mechanism was well explained with the help of quenching rate constant values.

d) Complexes **1** and **2** are docked with DNA as well as BSA and HSA by molecular docking study to recognize the orientations of **1** and **2** in the binding site of both DNA and protein molecules. Finally, the binding of **1** and **2** with DNA was found to be moderate in nature and was confirmed by molecular docking study. Complex **1** forms one hydrogen bond and seven hydrophobic interactions with the CDOCKER interaction energy of -47.0462 kcal/mol whereas complex **2** gains its stability by forming five hydrogen bond and two hydrophobic interactions with CDOCKER interaction energy of - 45.8947kcal/mol. It was observed from the binding energy

study that the complex **1** has the higher binding affinity than that of the complex **2** molecule.

e) Both complexes **1** and **2** have greater anti-proliferative and anti-apoptotic activity in respect to their controls. Complexes **1** and **2** cause significant increase in sub-G0 phase on AGS and A549 in respect to their control cells. In case of apoptosis, both complexes **1** and **2** have anti-apoptotic activity and results also suggest that complex **2** is better anti-apoptotic drug than complex **1**.

Conflict of interest

There are no conflicts of interest to declare.

Acknowledgements

N. Biswas acknowledges CSIR, New Delhi, Govt. of India, for awarding junior research fellowship (Project No: 01/2537/11- EMR - II). C. Roy Choudhury acknowledges DST- FIST (Project No. SR/FST/CSI-246/2012) New Delhi, Govt. of India for instrumental support under capital heads.

Appendix A. Supplementary data

CCDC 1011057 and 1011056 contains the supplementary crystallographic data for complexes **1** and **2** respectively. These data can be obtained free of charge via http://www.ccdc.cam.ac.uk/conts/retrieving.html, or from the Cambridge Crystallographic Data Centre, 12 Union Road, Cambridge CB2 1EZ, UK; fax: (+44) 1223-336-033; or e-mail:

deposit@ccdc.cam.ac.uk. Supplementary data associated with this article can be found, in the online version, at http://

References

Ainscough, E. W., Brodie, A. M., Ranford, J. D., Waters, & Murray, K. S. (1992). The reaction of the pyrophosphate ion with the antitumour complex [{CuL(CH_3COO)}$_2$] (HL=2-formylpyridine thiosemicarbazone) and the single-crystal X-ray structure of [$(CuL)_4P_2O_7$]·$n$$H_2O$. *Inorganica Chimica Acta*, *197* (1), 107-115.

Ainscough, E. W., Brodie, A.M., Ranford, J. D., & Waters, J. M. (1997). Reaction of anionic oxygen donors with the antitumourcopper(II)–pyridine-2-carbaldehydethiosemicarbazone (HL) system and the crystal structure of [{Cu(HL)(H_2PO_4)}$_2$][H_2PO_4]$_2$·$2H_3PO_4$·$2H_2O$. Journal of the Chemical Society, *Dalton Transactions*, *0* (7), 1251-1256.

Ainscough, E. W., Brodie, A. M., Ranford, J. D., & Waters. J. M. (1991). Preparation and characterization of complexes of the antitumour copper(II) 2-formylpyridine thiosemicarbazone (HL) system and the single-crystal X-ray structures of [{Cu(HL)(CF_3CO_2)}$_2$][CF_3CO_2]$_2$ and [Cu(HL)(H_2O)(CLO_4)$_2$]·$2H_2O$. Journal of the Chemical Society, *Dalton Transactions*, *0* (8), 2125-2131.

Accelrys Discovery Studio Visualiser v 3.5.0.12158, Accelrys Software Inc, San Diego.

Alagesan, M., Sathyadevi, P., Krishnamoorthy, P., Bhuvanesh, N. S. P., & Dharmaraj, N. (2014). DMSO containing ruthenium(II) hydrazone complexes: *in vitro*evaluation of biomolecular interaction and anticancer activity. *Dalton Transactions*, *43* (42), 15829-15840.

Biswas, N., Khanra, S., Sarkar, A., Bhattacharjee, S., Mandal, D. P., Chaudhuri, A.,

Chakraborty, S., & Choudhury, C. R. (2017). One new azido bridged dinuclear copper(II) thiosemicarbazide complex: synthesis, DNA/protein binding, molecular docking study and cytotoxicity activity. *New Journal of Chemistry*, *41* (21) 12996-13011.

Bell, C. F., & Theochars, C.R. (1987). Structure of the antitumour agent di-μ-acetato-(*O*)-bis[(2-pyridinecarbaldehyde thiosemicarbazonato)copper(II)]. *Acta Crystallographica. Section C*, *43* (1), 26-29.

Bingham, A. G., Bogge, H., Muller, A., Ainscough, E. W., & Brodie, A. M. (1987). Synthetic, spectroscopic, and *X*-ray crystallographic studies on binuclear copper(II) complexes with a tridentate NNS-bonding 2-formylpyridine thiosemicarbazone ligand. The characterization of both neutral and deprotonated co-ordinated ligand structures. *Journal of the Chemical Society, Dalton Transactions*, (3), 493-499.

Brissos, R., Ramos, D., Lima, J. C., Mihan, F. Y., Borràs, M., Lapuente, J., Cort, A. D., & Rodríguez, L. (2013). Luminescent zinc salophen derivatives: cytotoxicity assessment and action mechanism studies.*New Journal of Chemistry*, *37* (4) 1046-1055.

Bruker 2000, SADABS, SMART and SAINT. Bruker AXS Inc., Madison, isconsin, USA, 2008.

Barve, A., Kumbhar, A., Bhat, M., Joshi, B., Butcher, R., Sonawane, U., & Joshi, R. (2009). Mixed-Ligand Copper(II) Maltolate Complexes: Synthesis, Characterization, DNA Binding and Cleavage, and Cytotoxicity. *Inorganic Chemistry*, *48* (19), 9120-9132.

Baguley, B. C., & Lebret, M. L. (1984). Quenching of DNA-ethidium fluorescence by amsacrine and other antitumor agents: a possible electron-transfer effect. *Biochemistry*, *23* (5), 937-943.

Banerjee, S., Mondal, S., Sen, S., Das, S., Hughes, D. L., Rizzoli, C., Desplanches, C., Mandal, C., & Mitra, S. (2009). Four new dinuclear Cu(II) hydrazone complexes using various organic spacers: syntheses, crystal structures, DNA binding and cleavage

studies and selective cell inhibitory effect towards leukemic and normal lymphocytes. *Dalton Transactions*, (34), 6849-6860.

Chen, J., Wang, X., Shao, Y., Zhu, J., Zhu, Y., Li, Y., Xu, Q., & Guo. Z. (2007). A Trinuclear Copper(II) Complex of 2,4,6-Tris(di-2-pyridylamine)-1,3,5-triazine Shows Prominent DNA Cleavage Activity. *Inorganic Chemistry*, *46* (8), 3306-3312.

Chew, S. T., Lo, K. M., Sinniah, S. K., Sim, K. S., & Tan, K. W. (2014). Synthesis, characterization and biological evaluation of cationic hydrazone copper complexes with diverse diimine co-ligands. *RSC Adv*ances, *4* (106), 61232-61247.

Chitrapriya, N., Kamatchi, T. S., Zeller, M., Lee, H., & Natarajan, K. (2011). Synthesis, spectroscopic, crystal structure and DNA binding of Ru(II) complexes with 2-hydroxy-benzoic acid [1-(4-hydroxy-6-methyl-2-oxo-2H-pyran-3-yl)-ethylidene]-hydrazide. *Spectrochimica Acta Part A, 81* (1), 128-134.

Chauhan, M., Banerjee, K., & Arjmand, F. (2007). DNA Binding Studies of Novel Copper(II) Complexes Containing L-Tryptophan as Chiral Auxiliary: In Vitro Antitumor Activity of Cu−Sn_2Complex in Human Neuroblastoma Cells. *Inorganic Chemistry*, *46* (8), 3072-3082.

Chanphai, P., & Tajmir-Riahi, H.A. (2017). DNA binding to folic acid-chitosan nanoconjugates. *Journal of Biomolecular Structure & Dynamics*, doi: 10.1080/07391102.2017.1371078

Dyson, P. J., & Sava, G. (2006). Metal-based antitumour drugs in the post genomic era. *Dalton Transactions*, *0* (16), 1929-1933.

Das, M., Nasani, R., Saha, M., Mobin, S.M., & Mukhopadhyay, S. (2015). Nickel(II) complexes with a flexible piperazinyl moiety: studies on DNA and protein binding and catecholase like properties. *Dalton Transactions*, *44* (5), 299-2310.

Efhimiadou, E. K., Thomadaki, H., Sanakis, Y., Raptopoulou, C. P., Katsaros, N., Scorilas,

A., Karaliota, A., & Psomas, G. (2007). Structure and biological properties of the copper(II) complex with the quinolone antibacterial drug *N*-propyl-norfloxacin and 2,2′-bipyridine. *Journal of Inorganic Biochem*istry, *101* (1), 64-73.

Eftink, M. R., & Ghiron, C. A. (1976). Fluorescence quenching of indole and model micelle systems. *The Journal of Physical Chemistry*, *80* (5), 486-493.

Eftink, M. R., (1991). Fluorescence Quenching Reaction: Probing Biological Macromolecular Structures, Biophysical and Biochemical Aspects of Fluorescence Spectroscopy, Plenum Press, New York.

Feller, S. E., & Mackerell, A. D. (2000). An Improved Empirical Potential Energy Function for Molecular Simulations of Phospholipids. *Journal of Physical Chemistry B*, *104* (31), 7510-7515.

Fu, X. -B., Liu, D. -D., Lin, Y., Hu, W., Mao, Z. -W., & Le, X.-Y. (2014). Water-soluble DNA minor groove binders as potential chemotherapeutic agents: synthesis, characterization, DNA binding and cleavage, antioxidation, cytotoxicity and HSA interactions. *Dalton Transactions*, *43* (23), 8721-8737.

Grau, J., Brissos, R. F., -Uber, J. S., Caballero, A. B., Caubet, A., Roubeau, O., Gregório, L.K., -Tomásc, R. P., & Gamez, P. (2015). The effect of potential supramolecular-bond promoters on the DNA-interacting abilities of copper–terpyridine compounds. *Dalton Transactions*, *44* (36), 16061-16072.

Ganguly, A., Chakraborty, P., Banerjee, K., & Choudhuri, S. K. (2014). The role of a Schiff base scaffold, N-(2-hydroxy acetophenone) glycinate-in overcoming multidrug resistance in cancer. *European Journal of Pharmaceutical Sciences*, *51*, 96-109.

Ghosh, R. D., Chakraborty, P., Banerjee, K., Adhikary, A., Sarkar, A., Chatterjee, M., Das, T., & Choudhuri, S. K. (2012). The molecular interaction of a copper chelate with human P-glycoprotein. *Molecular and Cellular Biochemistry*, *364* (1-2) 309-320.

Ganguly, A., Basu, S., Banerjee, K., Chakraborty, P., Sarkar, A., Chatterjee, M., & K. Chaudhuri, S. (2011). Redox active copper chelate overcomes multidrug resistance in T-lymphoblastic leukemia cell by triggering apoptosis. *Moleculal BioSystems, 7* (5), 1701-1712.

Guo, Z., & Sadler, P. J. (1999). Metals in Medicine. *Angewandte Chemie International Edition*, *38* (11), 1512-1531.

Garcia-Tojal, J., Urtiaga, M. K., Cortes, R., Lezama, L., Rojo, T., & Arriortua, M. I. (1994). Synthesis, structure, spectroscopic and magnetic properties of two copper(II) dimers containing pyridine-2-carbaldehyde thiosemicarbazonate (L), [{CuL(X)}$_2$](X = Cl or Br). *Journal of the Chemical Society, Dalton Transactions,* (15), 2233-2238.

Garcia-Tojal, J., Lezama, L., Pizarro, J. L., Insausti, M., Arriortua, M. I., & Rojo, T. (1999). Spectroscopic and magnetic properties of copper(II) complexes derived from pyridine-2-carbaldehyde thiosemicarbazone. Structures of [Cu(NO_3)($C_7H_8N_4S$)(H_2O)](NO_3) and [{Cu(NCS)($C_7H_7N_4S$)}$_2$]. *Polyhedron*, *18* (27), 3703-3711.

Garcia-Tojal, J., Garcia-Jaca, J., Cortes, R., Rojo, T., Urtiaga, M. K., & Arrortua, M. I. (1996). Synthesis and spectroscopic properties of two pyridine-2-carbaldehyde thiosemicarbazonecopper(II) compounds: [CuX_2($C_7H_8N_4S$)]·H_2O (X = Br, Cl). Crystal structure of the bromo complex. *Inorganica Chimica Acta*, *249* (1), 25-32.

Giannicchi, I., Brissos, R., Ramos, D., Lapuente, J., Lima, J. C., Cort, A. D., & Rodríguez, L. (2013). Substituent Effects on the Biological Properties of Zn-Salophen Complexes. *Inorganic Chemistry, 52* (16) 9245-9253.

Glaser, T., Lügger, T., & Fröhlich, R. (2004). Synthesis, Crystal Structures, and Magnetic Properties of a Mono- and a Dinuclear Copper(II) Complex of the 2,4,6-Tris(2-pyridyl)-1,3,5-triazine Ligand. *European Journal of Inorganic Chemistry, 2004* (2) 394-400.

Gupta, R. K., Sharma, G., Pandey, R., Kumar, A., Koch, B., Li, P. Z., Xu, Q., & Pandey, D. S. (2013). DNA/Protein Binding, Molecular Docking, and in Vitro Anticancer Activity of Some Thioether-Dipyrrinato Complexes. *Inorganic Chemistry*, *52* (24), 13984-13996.

Gabbay, E. J., Scofield, R. E., & Baxter, C. S. (1973). Topography of nucleic acid helixes in solution. XXIX. Steric effects on the intercalation of aromatic cations to deoxyribonucleic acid. *Journal of the American Chemical Society*, *95* (23), 7850-7857.

Ganeshpandian, M., Loganathan, R., Ramakrishnan, S., Riyasdeen, A., Akbarsha, M. A., & Palaniandavar, M. (2013). Interaction of mixed ligand copper(II) complexes with CT DNA and BSA: Effect of primary ligand hydrophobicity on DNA and protein binding and cleavage and anticancer activities. *Polyhedron*, *52*, 924-938.

Haribabu, J., Jeyalakshmi, K., Arun, Y., Bhuvanesh, N.S.P., Perumalm, P.T., & Karvembu, R. (2015). Synthesis, DNA/protein binding, molecular docking, DNA cleavage and *in vitro* anticancer activity of nickel(II) bis(thiosemicarbazone) complexes. *RSC Adv*ances, *5* (57), 46031-46049.

Ingle, S. A., Kate, A. N., Khumbhar, A. A., Khan, A. A., Rao, S. S., & Gejji, S.P. (2015). Synthesis and biological evaluation of copper(II) pyrenethiosemicarbazone. *RSC. Advances*, *5*(59), 47476-47487.

Indumathy, R., Radhika, S., Kanthimathi, M., Weyhermuller, T., & Nair, B. U. (2007). Cobalt complexes of terpyridine ligand: Crystal structure and photocleavage of DNA. *Journal Inorganic Biochemistry*, *101* (3), 434-443.

Jaividhya, P., Ganeshpandian, M., Dhivya, R., Akbarsha, M. A., & Palaniandavar, M. (2015). Fluorescent mixed ligand copper(II) complexes of anthracene-appended Schiff bases: studies on DNA binding, nuclease activity and cytotoxicity. *Dalton Transactions*, *44* (26), 11997-12010.

Jeyalakshmi, K., Arun, Y., Bhuvanesh, N. S.P., Perumal, P. T., Sreekanth, A., & Karvembu,

R. (2015). DNA/protein binding, DNA cleavage, cytotoxicity, superoxide radical scavenging and molecular docking studies of copper(II) complexes containing *N*-benzyl-*N′*-aryl-*N″*-benzoylguanidine ligands. *Inorganic Chemistry Frontiers*, *2* (8), 780-798.

Jafari, F., Samadi, S., Nowroozi, A., Sadrjavadi, K., Moradi, S., Ashrafi-Kooshk, M. R., & Shahlaei, M. (2017). Experimental and Computational studies on the Binding of Diazinon to Human Serum Albumin. *Journal of Biomolecular Structure and Dynamics*, *36* (6) 1490-1510.

Kathiresan, S., Mugesh, S., Murugan, M., & Annaraj, J. (2017). Mixed-ligand copper(II) Schiff base complexes: the vital role of co-ligands in DNA/protein interactions and cytotoxicity. *New Journal of Chemistry*, *41*(3), 1267-1283.

Kumar, R. R., Subarkhan, M. K. M., & Ramesh, R. (2015). Synthesis and structure of nickel(II) thiocarboxamide complexes: effect of ligand substitutions on DNA/protein binding, antioxidant and cytotoxicity. *RSC Advances*, *5* (58), 46760-46773.

Kalaivani, P., Prabhakaran, R., Vaishnavi, E., Rueffer, T., Lang, H., Poornima, P., Renganathan, R., Vijaya Padmad, V., & Natarajan, K. (2014). Synthesis, structure, DNA/protein binding and *in vitro* cytotoxicity of new ruthenium metallates. *Inorganic Chemistry Frontiers*, *1* (4), 311-324.

Krishnamoorthy, P., Sathyadevi, P., Cowley, A. H., Butorac, R. R., & Dharmaraj, N. (2011).Evaluation of DNA binding, DNA cleavage, protein binding and *in vitro* cytotoxic activities of bivalent transition metal hydrazone complexes. *European Journal of Medicinal Chemistry*, *46* (8) 3376-3387.

Kumar, P., Gorai, S., Santra, M. K., Mondal, B., & Manna, D. (2012). Mechanochemical and solution synthesis, X-ray structure and IR and ^{31}P solid state NMRspectroscopic studies of copper(I) thiocyanateadducts with bulky monodentate tertiary phosphineligands. *Dalton Transactions*, *41* (25), 7573-7581.

Krishnamoorthy, P., Sathyadevi, P., Butorac, R. R., Cowley, A. H., Bhuvanesh, N. S. P., & Dharmaraj, N. (2012). Copper(I) and nickel(II) complexes with 1 : 1 *vs.* 1 : 2 coordination of ferrocenyl hydrazone ligands: Do the geometry and composition of complexes affect DNA binding/cleavage, protein binding, antioxidant and cytotoxic activities? *Dalton Transactions*, *41* (15), 4423-4436.

Kalaivani, P., Prabhakaran, R., Dallemer, F., Vaishnavi, E., Poornima, P., Vijaya Padma, V., Renganathan, R., & Natarajan, K. (2014). Synthesis, structural characterization, DNA/Protein binding and *in vitro* cytotoxicity of isomeric ruthenium carbonyl complexes. *Journal of Organometallic Chemistry*, *762*, 67-80.

Kalaivani, P., Saranya, S., Poornima, P., Prabhakaran, R., Dallemer, F., Vijaya Padma, V., & Natarajan, K. (2014). Biological evaluation of new nickel(II) metallates: Synthesis, DNA/protein binding and mitochondrial mediated apoptosis in human lung cancer cells (A549) via ROS hypergeneration and depletion of cellular antioxidant pool. *European Journal of Medicinal Chemistry*, *82*, 584-599.

Kosiha, A., Parthiban, C., Ciattini, S., Chelazzi, L., & Elango, K. P. (2017). Metal complexes of naphthoquinone based ligand: Synthesis, characterization, protein binding, DNA binding/cleavage and cytotoxicity studies. *Journal of Biomolecular Structure and Dynamics*, doi: 10.1080/ 07391102.2017.1413423

Lian, W. -J., Wang, X. -T., Xie, C. -Z., Tian, H., Song, X. -Q., Pan, H. -T., Qiao, X., & Xu, J. -Y. (2016). Mixed-ligand copper(II) Schiff base complexes: the role of the co-ligand in DNA binding, DNA cleavage, protein binding and cytotoxicity. *Dalton Transactions*, *45*(22), 9073-9087.

Lu, J., Sun, Q., Li, J. -L., Jiang, L., Gu, W., Liu, X., Tian, J. -L., & Yan, S. -P. (2014). Two water-soluble copper(II) complexes: Synthesis, characterization, DNA cleavage, protein binding activities and in vitro anticancer activity studies. *Journal of Inorganic*

*Biochem*istry, *137*, 46-56.

Lobana, T. S., Bawa, G., Hundal, G., & Zeller, M. (2008). The influence of substituents at C2 carbon atom of thiosemicarbazones {R(H)C^2=N^3-N^2(H)-C^1(=S)- N^1H_2} on their dentacy in PtII/PdII complexes: synthesis, spectroscopy, and crystal structures. *Zeitschrift für Anorganische Und Allgemeine Chemie*, *634* (5) 931-937.

Lobana, T. S., Bawa, G., Castineiras, A., Butcher, R. J., & Zeller, M. (2008). Bis(diphenylphosphino)methane Induces Unusual Cyclometalation of Thiophene and Phenyl Rings (R) at the C^2 Carbon of Thiosemicarbazones {R-C^2(H) = N^3-N^2 H-C(=S)-N^1H_2} in Ruthenium(II) Complexes. *Organometallics*, *27* (2), 175-180.

Lobana, T. S., Rekha, Butcher, R. J., Castineiras, A., Bermejo, E., & Bharatam, P. V. (2006). Bonding Trends of Thiosemicarbazones in Mononuclear and Dinuclear Copper(I) Complexes: Syntheses, Structures, and Theoretical Aspects. *Inorganic Chemistry*, *45* (4), 1535-1542.

Lobana, T.S., Khanna, S., Hundal, G., Kaur, P., Thakur, B., Attri, S., & Butcher, R.J. (2009). Coinage metal derivatives of salicylaldehyde thiosemicarbazones: Synthesis, structures, bond isomerism and H-bonded networks. *Polyhedron*, *28* (8), 1583-1593.

Lobana, T. S., Kumari, P., & Butcher, R. J. (2008). Cyclopentanone thiosemicarbazone (Hcptsc) induces a new bonding pattern in $(Ph_3P)Cu(\mu\text{-}Br)(\mu_3\text{-}S,N\text{–}Hcptsc)CuBr(PPh_3)$ dimer. *Inorganic Chemistry Communications*, *11* (1), 11-14.

Lecloux, D. D., Davydov, R., & Lippard, S. J. (1998). Synthesis and Characterization of Spin-Delocalized Carboxylate-Bridged Cu(I)−Cu(II) Mixed-Valence Complexes Having Only Oxygen Donor Ligands. *Journal of the American Chemical Society*, *120* (27) 6810-6811.

Li, T. R., Yang, Z. Y., Wang, B. D., & Qin, D. D. (2008). Synthesis, characterization, antioxidant activity and DNA-binding studies of two rare earth(III) complexes with

naringenin-2-hydroxy benzoyl hydrazone ligand. *European Journal of Medicinal Chemistry*, *43* (8), 1688-1695.

Lakowicz, J. R., & Webber, G. (1973). Quenching of fluorescence by oxygen. A probe for structural fluctuations in macromolecules. *Biochemistry*, *12* (21), 4161-4170;

Lepecq, J. B., & Paoletti, C. (1967). A fluorescent complex between ethidium bromide and nucleic acids. Physical-chemical characterization. *Journal of Molecular Biol*ogy, *27* (1), 87-106.

Lakowicz, J. R., (2013). Principles of fluorescence spectroscopy, Springer Science & Business Media.

Leone, A. M., Tibodeau, J. D., Bull, S. H., Feldberg, S. W., Thorp, H. H., & Murray, R. W. (2003). Ion Atmosphere Relaxation and Percolative Electron Transfer in Co Bipyridine DNA Molten Salts. *Journal of the American Chemical Society*, *125* (22), 6784-6790.

Li, F. -H., Zhao, G. H., & Wu, H. X. (2006). Synthesis, characterization and biological activity of lanthanum(III) complexes containing 2-methylene–1,10-phenanthroline units bridged by aliphatic diamines. *Journal of Inorganic Biochemistry*, *100* (1), 36-43.

Lo, S. M. -F., Chui, S. S. -Y., Shek, L. -Y., Lin, Z. -Y., Zhang, X. -X., Wen, G.- H., & Williams, I.D. (2000). Solvothermal Synthesis of a Stable Coordination Polymer with Copper-I−Copper-II Dimer Units: $[Cu_4\{1,4\text{-}C_6H_4(COO)_2\}_3(4,4'\text{-bipy})_2]_n$. *Journal of the American Chemical Society*, *122* (26), 6293-6294.

Mandegani, Z., Asadi, M., Karbalaei-Heidari, H. R., Rastegari, B., & Asadi, Z. (2016). Synthesis, characterization, DNA binding, cleavage activity, cytotoxicity and molecular docking of new nano water-soluble $[M(5\text{-}CH_2PPh_3\text{-}3,4\text{-salpyr})](ClO_4)_2$ (M = Ni, Zn) complexes. *Dalton Transactions*, *45* (15), 6592-6611.

Muralisankar, M., Sujith, S., Bhuvanesh, N. S. P., & Sreekanth, A. (2016). Synthesis and crystal structure of new monometallic and bimetallic copper(II) complexes with N-

substituted isatin thiosemicarbazone ligands: Effects of the complexes on DNA/protein-binding property, DNA cleavage study and *in vitro* anticancer activity. *Polyhedron*, *118*, 103-117.

Manikandan, R., Chitrapriya, N., Jang, Y. J., & Viswanathamurth, P. (2013). Evaluation of DNA-binding, radical scavenging and cytotoxic activity of five coordinated Cd(II) complexes containing 2-acetylpyridine-N^4-substituted thiosemicarbazone. *RSC. Advances*, *3* (29), 11647-11657.

Mackerell, A. D., Bashford, D., Bellott, M., Dunbrack, R. L., Evanseck, J. D., & Karplus, M. (1998). All-Atom Empirical Potential for Molecular Modeling and Dynamics Studies of Proteins. *Journal of Physical Chemistry B, 102* (18), 3586-3616.

Mistri, S., Puschmann, H., & Manna, S. C. (2016). DNA/protein binding, cytotoxicity and catecholase activity studies of a piperazinyl moiety ligand based nickel(II) complex. *Polyhedron*, *115*, 155-163.

Mancin, F., Scrimin, P., Tecilla, P., & Tonellato, U. (2005). Artificial metallonucleases. *Chem. Commun*, *0* (20), 2540-2548.

Nanjundan, N., Butcher, R. J., Jasinski, J. P., Velmurugan, K., Nandhakumar, R., Balakumaran, M. D., Kalaichelvan, P. T., Gnanasoundari, V.G., & Narayanasamy, R. (2017). Synthesis, crystal structure, biomolecular interactions and anticancer properties of Ni(II), Cu(II) and Zn(II) complexes bearing S-allyldithiocarbazate. *Inorganica Chimica Acta, Part 1*, *455*, 283-297.

Najjar, R., & Espósito, B. P. (2002). Interactions of antitumoral platinum-group metallodrugs with albumin. *Coordination Chemistry Reviews*, *232* (1-2), 137-150.

Orvig, C., & Abrams, M. J. (1999). Medicinal Inorganic Chemistry: Introduction. *Chemical Reviews*, *99* (9), 2201-2204.

Patra, A., Sen, T. K., Ghorai, A., Musie, G. T., Mandal, S. K., Ghosh, U., & Ber, M. (2013).

Synthesis, Structure, Spectroscopic Characterization, and Protein Binding Affinity of New Water-Soluble Hetero- and Homometallic Tetranuclear [$Cu^{II}_2Zn^{II}_2$] and [Cu^{II}_4] Clusters. *Inorganic Chemistry*, *52*(6), 2880-2890.

Prabhakaran, R., Renukadevi, S. V., Karvembu, R., Huang, R., Mautz, J., Huttner, R., Subhaskumar, G., & Natarajan, K. (2008). Structural and biological studies of mononuclear palladium(II) complexes containing *N*-substituted thiosemicarbazones. *European Journal of Medicinal Chemistry*, *43* (2) 268-273.

Prabhakaran, R., Huang, R., Renukadevi, S. V., Karvembu, R., Zeller, M., & Natarajan, K. (2008). Coordination behaviour of ferrocenylthiosemicarbazone in a novel hetero trinuclear nickel(II) complex: Synthesis, spectral, electrochemistry and X-ray crystallography. *Inorganica Chimica Acta*, *361* (8), 2547-2552.

Pradeepa, S. M., Kumar, B. V., Priyadarsini, K. I., Barik, A., Jayakumar, S., & B. Naik, H. S. (2015). Synthesis and characterization of cobalt(II), nickel(II) and copper(II)-based potential photosensitizers: Evaluation of their DNA binding profile, cleavage and photocytotoxicity. *Inorganica Chimica Acta*, *428*, 138-146.

Poornima, S., Gunasekaran, K., & Kandaswamy, M. (2015). Nuclease activity and interaction studies of unsymmetrical binuclear Ni(II) complexes with CT-DNA and BSA. *Dalton Transactions*, *44* (37), 16361- 16371.

Patra, D., Paul, S., Sepay, N., Kundu, R., & Ghosh, T. (2017). Structure-activity relationship on DNA binding and anticancer activities of a family of mixed ligand oxidovanadium(V) hydrazone complexes. *Journal of Biomolecular Structure and Dynamics*, doi: 10.1080/ 07391102.2017.1409652

Rambabu, A., Kumar, M. P., Tejaswi, S., Vamsikrishna, N., & Shivaraj. (2016). DNA interaction, antimicrobial studies of newly synthesized copper (II) complexes with 2-

amino-6-(trifluoromethoxy)benzothiazole Schiff base ligands. *Journal of Photochemistry and Photobiology B: Biology*. *165*, 147-156.

Reichmann, M., Rice, S., Thomas, C., & Doty, P. (1954). A Further Examination of the Molecular Weight and Size of Desoxypentose Nucleic Acid. *Journal of American Chemical Society*, *76* (11), 3047-3053.

Raman, N., & Jeyamurugan, R. (2009). Synthesis, characterization, and DNA interaction of mononuclear copper(II) and zinc(II) complexes having a hard-soft NS donor ligand. *Journal of Coordination Chemistry*, *62* (14), 2375-2387.

Reddy, P. R., Shilpa, A., Raju, N., & Raghavaiah, P. (2011). Synthesis, structure, DNA binding and cleavage properties of ternary amino acid Schiff base-phen/bipy Cu(II) complexes. *Journal of Inorganic Biochemistry*, *105* (12), 1603-1612.

Rajalakshmi, S., Kiran, M. S., Vaidyanathan, V. G., Singam, E. R. A., Subramaniam, V., & Nair, B.U. (2013). Investigation of nuclease, proteolytic and antiproliferative effects of copper(II) complexes of thiophenylmethanamine derivatives. *European Journal of Medicinal Chemistry*, *70*, 280-293.

Raja, D. S., Paramaguru, G., Bhuvanesh, N. S. P., Reibenspies, J. H., Renganathan, R., & Natarajan, K. (2011). Effect of terminal N-substitution in 2-oxo-1,2-dihydroquinoline-3-carbaldehydethiosemicarbazones on the mode of coordination, structure, interaction with protein, radical scavenging and cytotoxic activity of copper(II) complexes. *Dalton Transactions*, *40* (17), 4548-4559.

Suntharalingam, K., Hunt, D. J., Duarte, A. A., White, A. J., Mann, D. J., & Vilar, R. (2012). A Tri-copper(II) Complex Displaying DNA-Cleaving Properties and Antiproliferative Activity against Cancer Cells. *Chemistry: A European Journal*, *18* (47), 15133-15141.

Singh, N. K., & Singh, S. B. (2001). Synthesis, characterization and biological properties of

manganese(II), cobalt(II), nickel(II), copper(II), zinc(II), chromium(III) and iron(III) complexes with a new thiosemicarbazide derivative. *Indian Journal of Chemistry*, 2001, *40A*, 1070-1075.

Sheldrick, G. M. (2008). A short history of SHELX. Acta Crystallographica Section A: *64*, 112-122.

Sreeja, P. B., Kurup, M. R. P., Kishore, A., & Jasmin, C. (2004). Spectral characterization, X-ray structure and biological investigations of copper(II) ternary complexes of 2-hydroxyacetophenone 4-hydroxybenzoic acid hydrazone and heterocyclic bases. *Polyhedron*, *23* (4), 575-581.

Sathyadevi, P., Krishnamoorthy, P., Alagesan, M., Thanigaimani, K., Muthiah, P. T., & Dharmaraj, N. (2012). Synthesis, crystal structure, electrochemistry and studies on protein binding, antioxidant and biocidal activities of Ni(II) and Co(II) hydrazone complexes. *Polyhedron*, *31* (1), 294-306.

Sathyadevi, P., Krishnamoorthy, P., Butorac, R. R., Cowley, A. H., & Dharmaraj, N. (2012). Synthesis of novel heterobimetallic copper(I) hydrazone Schiff base complexes: A comparative study on the effect of heterocyclic hydrazides towards interaction with DNA/protein, free radical scavenging and cytotoxicity. *Metallomics*, *4* (5), 498-511.

Saswati, Chakraborty, A., Dash, S. P., Panda, A. K., Acharyya, R., Biswas, A., Mukhopadhyay, S., Bhutia, S. K., Crochet, A., Patil, Y. P., Nethajie, M., & Dinda, R. (2015). Synthesis, X-ray structure and *in vitro*cytotoxicity studies of Cu(I/II) complexes of thiosemicarbazone: special emphasis on their interactions with DNA. *Dalton Transactions*, *44* (13), 6140-6157.

Srinivasan, S., Annaraj, J., & Athappan, P. (2005). Spectral and redox studies on mixed ligand complexes of cobalt(III) phenanthroline/bipyridyl and benzoylhydrazones, their DNA binding and antimicrobial activity. *Journal of Inorganic Biochemistry*, *99* (3),

876-882.

Sathyadevi, P., Krishnamoorthy, P., Butorac, R. R., Cowley, A. H., Bhuvanesh, N. S. P., & Dharmaraj, N. (2011). Effect of substitution and planarity of the ligand on DNA/BSA interaction, free radical scavenging and cytotoxicity of diamagnetic Ni(II) complexes: A systematic investigation. *Dalton Transactions*, *40* (38), 9690-9702.

Samari, F., Hemmateenejad, B., Shamsipur, M., Rashidi, M., & Samouei, H. (2012). Affinity of Two Novel Five-Coordinated Anticancer Pt(II) Complexes to Human and Bovine Serum Albumins: A Spectroscopic Approach. *Inorganic Chemistry*, *51* (6), 3454-3464.

Singh, N., Pagariya, D., Jain, S., Naik, S., & Kishore, N. (2017). Interaction of copper (II) complexes by bovine serum albumin: spectroscopic and calorimetric insights. *Journal of Biomolecular Structure and Dynamics*, doi: 10.1080/07391102.2017.1355848

Salci, A., & Toprak, M. (2015). Spectroscopic investigations on the binding of Pyronin Y to human serum albumin. *Journal of Biomolecular Structure and Dynamics*. *35* (1) 8-16.

Tabassum, S., Asim, A., Arjmand, F., Afzal, M., & Bagchi., V. (2012). Synthesis and characterization of copper(II) and zinc(II)-based potential chemotherapeutic compounds: Their biological evaluation *viz*. DNA binding profile, cleavage and antimicrobial activity. *European Journal of Medicinal Chemistry*, *58*, 308-316.

Tai, A. W., Lien, E. J., Lai, M. M., & Khwaja, T. A. (1984). Novel N-hydroxyguanidine derivatives as anticancer and antiviral agents. *Journal of Medicinal Chemistry*, *27* (2), 236-238.

Tjioe, L., Meininger, A., Joshi, T., Spiccia, L., & Graham, B. (2011). Efficient Plasmid

DNA Cleavage by Copper(II) Complexes of 1,4,7-Triazacyclononane Ligands Featuring Xylyl-Linked Guanidinium Groups. *Inorganic Chemistry*, *50* (10), 4327-4339.

Vafazadeh, R., Namazian, M., Chavoshiyan, M., Willis, A. C., & Carr. P. D. (2017). Synthesis, X-Ray Structural Characterization, and DFT Calculations of Binuclear Mixed-Ligand Copper(II) Complexes Containing Diamine, Acetate and Methacrylate Ligands. *Acta Chimica Sovenica*, *64* (3), 613-620.

Wang, P. H., Keck, J. G., Lien, E. J., & Lai, M. M. (1990). Design, synthesis, testing, and quantitative structure-activity relationship analysis of substituted salicylaldehyde Schiff bases of 1-amino-3-hydroxyguanidine tosylate as new antiviral agents against coronavirus *Journal of Medicinal Chemistry*, *33* (2), 608-614.

Wu, G., Robertson, D. H., Brooks III, C. L., & Vieth, M. (2003). Detailed Analysis of Grid-Based Molecular Docking: A Case Study of CDOCKER - A CHARMm-Based MD Docking Algorithm. *Journal of Computational Chemistry*, *24* (13), 1549-1562.

Wolfe, A., Shimer, G. H., & Meehan, T. (1987). Polycyclic aromatic hydrocarbons physically intercalate into duplex regions of denatured DNA. *Biochemistry*, *26* (20), 6392-6396.

Wang, Y. -Q, Zhang, H. -M, Zhang, G. -C, Tao, W. -H, & Tang, S. -H. (2007). Interaction of the flavonoid hesperidin with bovine serum albumin: A fluorescence quenching study. *Journal of Luminescence*, *126* (1), 211-218.

Yilmaz, V. T., Icsel, C., Suyunova, F., Aygun, M., Cevatemre, B., & Ulukaya, E. (2017). Synthesis, structures, DNA/protein binding, molecular docking, anticancer activity and ROS generation of Ni(II), Cu(II) and Zn(II) 5,5-diethylbarbiturate complexes with bis(2-pyridylmethyl)amine and terpyridine *New Journal of Chem*isrty, *41* (16), 8092-8106.

Zhang, X. -M., Tong, M.-L., Gong, M. -L., Lee, H.-K., Luo, L., Li, K. -F., Tong, Y. -X.,

& Chen, X. -M. (2002). Syntheses, Crystal Structures, and Physical Properties of Dinuclear Copper(I) and Tetranuclear Mixed-Valence Copper(I,II) Complexes with Hydroxylated Bipyridyl-Like Ligands. *Chemistry A European Journal, 8* (14), 3187-3194.

Zhao, G., Lin, H., Zhu, S., Sun, H., & Chen, Y. (1998). Dinuclear palladium(II) complexes containing two monofunctional $[Pd(en)(pyridine)Cl]^{+}$ units bridged by Se or S. Synthesis, characterization, cytotoxicity and kinetic studies of DNA-binding. *Journal Inorganic Biochemistry, 70* (3-4), 219-226.

Zhang, Y. -Z., Li, H. -R., Dai, J., Chen, W. -J., Zhang, J., & Liu, Y. (2010). Spectroscopic studies on the binding of cobalt (II) 1,10-phenanthtoline complex to bovine serum albumin. *Biological Trace Element Research, 135* (1-3), 136-152.

Zhou, H., Shi, X., Fan, Y., He, Z., Gu, W., Ye, L., & Meng, F. (2018). Interaction of Prussian blue nanoparticles with bovine serum albumin: a multi-spectroscopic approach. *Journal of Biomolecular Structure and Dynamics, 36* (1), 254-261.